

**Contract No:**

This document was prepared in conjunction with work accomplished under Contract No. 89303321CEM000080 with the U.S. Department of Energy (DOE) Office of Environmental Management (EM).

**Disclaimer:**

This work was prepared under an agreement with and funded by the U.S. Government. Neither the U.S. Government or its employees, nor any of its contractors, subcontractors or their employees, makes any express or implied:

- 1 ) warranty or assumes any legal liability for the accuracy, completeness, or for the use or results of such use of any information, product, or process disclosed; or
- 2 ) representation that such use or results of such use would not infringe privately owned rights; or
- 3) endorsement or recommendation of any specifically identified commercial product, process, or service.

Any views and opinions of authors expressed in this work do not necessarily state or reflect those of the United States Government, or its contractors, or subcontractors.



**Savannah River  
National Laboratory®**

A U.S. DEPARTMENT OF ENERGY NATIONAL LABORATORY • SAVANNAH RIVER SITE • AIKEN, SC

# **Flowsheet for the Neutralization of Accelerated Basin De-inventory (ABD) Material**

**K. M. L. Taylor-Pashow**

**E. K. Hansen**

**T. S. Rudisill**

**C. L. Trivelpiece**

June 2022

SRNL-STI-2022-00114, Revision 0

SRNL.DOE.GOV

## **DISCLAIMER**

This work was prepared under an agreement with and funded by the U.S. Government. Neither the U.S. Government or its employees, nor any of its contractors, subcontractors or their employees, makes any express or implied:

1. warranty or assumes any legal liability for the accuracy, completeness, or for the use or results of such use of any information, product, or process disclosed; or
2. representation that such use or results of such use would not infringe privately owned rights; or
3. endorsement or recommendation of any specifically identified commercial product, process, or service.

Any views and opinions of authors expressed in this work do not necessarily state or reflect those of the United States Government, or its contractors, or subcontractors.

**Printed in the United States of America**

**Prepared for  
U.S. Department of Energy**

**Keywords:** *ABD, neutralization, H-Canyon, Gd poison*

**Retention:** *Varies*

## **Flowsheet for the Neutralization of Accelerated Basin De-inventory (ABD) Material**

K. M. L. Taylor-Pashow  
E. K. Hansen  
T. S. Rudisill  
C. L. Trivelpiece

June 2022

---

Savannah River National Laboratory is operated by  
Battelle Savannah River Alliance for the U.S. Department  
of Energy under Contract No. 89303321CEM000080.



## REVIEWS AND APPROVALS

### AUTHORS:

---

K. M. L. Taylor-Pashow, Chemical Flowsheet Development	Date
--------------------------------------------------------	------

---

E. K. Hansen, Chemical Flowsheet Development	Date
----------------------------------------------	------

---

T. S. Rudisill, Actinide and Separations Science	Date
--------------------------------------------------	------

---

C. L. Trivelpiece, Applied Materials Research	Date
-----------------------------------------------	------

### TECHNICAL REVIEW:

---

T. C. Shehee, Separation Science and Engineering, Reviewed per E7 2.60	Date
------------------------------------------------------------------------	------

---

M. R. Poirier, Chemical Flowsheet Development, Reviewed per E7 2.60	Date
---------------------------------------------------------------------	------

### APPROVAL:

---

G. A. Morgan, Manager Chemical Flowsheet Development	Date
---------------------------------------------------------	------

---

F. M. Pennebaker, Director, Chemical Processing	Date
-------------------------------------------------	------

---

A. M. Hudlow, SRNS Materials Disposition Engineering	Date
------------------------------------------------------	------

## EXECUTIVE SUMMARY

Under the Accelerated Basin De-inventory (ABD) program H-Canyon will be dissolving aluminum spent nuclear fuel (ASNF) and then neutralizing that solution without performing head-end strike or uranium recovery operations. After dissolution in H-Canyon the material will be neutralized to a free hydroxide concentration of either 0.6 M or 1.2 M to meet the waste acceptance criteria for transfer to the SRS Concentration, Storage and Transfer Facility (CSTF). In order to ensure the material could be successfully neutralized and transferred, SRNL completed experiments with simulated H-Canyon dissolver solutions. Two bounding simulants were developed based on the expected compositions of ASNF to be dissolved, one containing only Gd as the neutron poison and one containing Fe as an additional poison.

The first simulant represented a batch of dissolver solution from dissolution of HFIR fuel after isotopic adjustment to 3 wt%  $^{235}\text{U}$  and poisoning with Gd at a ratio of 0.625:1 Gd: $^{235}\text{U}$ . The second simulant also represented a batch of dissolved HFIR fuel, adjusted to 3 wt%  $^{235}\text{U}$  enrichment, with Gd added at a ratio of 0.625:1, but also included the addition of Fe as a neutron poison at a ratio of 160:1 Fe: $^{239}\text{Pu}$  equivalent. Analysis of samples taken throughout the neutralization indicated the lowest Gd: $^{235}\text{U}$  ratio was observed at about the mid-point of the neutralization where the ratio was 0.549 in the solids. This ratio is still well within the safety limits based on the Nuclear Criticality Safety Evaluation (NCSE) performed to calculate the minimum critically safe Gd: $^{235}\text{U}$  ratio in an infinite system. The evaluation found this ratio to be 0.025 Gd: $^{235}\text{U}$  for all credible hydrogen to fissile atom ratios. Similar results were obtained for the simulant also containing Fe, where the minimum Gd: $^{235}\text{U}$  ratio observed was 0.552 in the solids.

Physical and rheological properties of the resulting neutralized simulants were also studied to provide the necessary data for performing flow calculations examining the transfer of neutralized slurry from H-Canyon to the CSTF. All endpoints had a final density above the 1.35 g/mL limit and therefore require further dilution at the end of the neutralization. For Simulant #1, the slurry can be successfully transferred after dilution to a density between 1.27 and 1.35 g/mL for both the 0.6 M and 1.2 M  $\text{OH}^-$  endpoints. To minimize water addition for Simulant #1, it is recommended to process at 1.35 g/mL. For Simulant #2, it was determined that flow will backup into the header if the pipe roughness is greater than 0.00015 ft for densities above 1.33 g/mL for the 0.6 M slurry. For Simulant #2 it is recommended to target final densities of 1.33 g/mL for the 0.6 M  $\text{OH}^-$  endpoint or 1.35 g/mL for the 1.2 M  $\text{OH}^-$  case if the transfer is non-Newtonian. If simulant #2 is transferred as a Newtonian fluid, target 1.25 g/mL for either the 0.6 M or 1.2 M  $\text{OH}^-$  endpoints, given densities higher than 1.25 g/mL should be treated as non-Newtonian. At 1.21 g/mL for Simulant #2, the critical velocity needed to maintain the  $\text{Na}_2\text{U}_2\text{O}_7$  particles in suspension exceeds that of the pipeline velocity, indicating settling could occur. If there is excessive buildup in the piping from previous transfers (e.g., pipe roughness greater than 0.00125 ft), backup into the 10" header will occur for either simulant. Flushing after transfers is recommended at or above 75 gpm.

In addition to the experimental studies, a literature survey and subsequent modeling evaluation were performed to determine the potential for seeding of sodium aluminosilicates following the neutralization that could lead to the formation of scale on the wall of the tank which may also contain uranium. Formation of aluminosilicate scale has previously been identified as an issue in the liquid waste processing activities at SRS, particularly in the evaporators where high-level waste containing high concentrations of Al and recycle water from the vitrification facility containing high concentrations of Si are combined and evaporated. The proposed mechanism for formation of the aluminosilicate scale in the SRS evaporators is the formation of a sodium aluminosilicate hydrogel precursor which converts to Zeolite-A under hydrothermal conditions at elevated temperature, and subsequently to nitrated-cancrinite/sodalite scale. Formation of the hydrogel requires a near 1:1 ratio of aluminate and silicate species, which is unlikely to occur in the H-Canyon process where the aluminate concentration will greatly exceed the silicate concentration. This in combination with the lower temperatures in the neutralization tanks indicate that the

formation of sodium aluminosilicate scale is not likely to occur in H-Canyon. Modeling of the first neutralized simulant from this work (Gd poison only) showed that the Si precipitated in the form of a small amount of a sodium aluminosilicate phase (natrolite,  $\text{Na}_2\text{Al}_2\text{Si}_2\text{O}_{10}\cdot 2\text{H}_2\text{O}$ ) that formed just after the equivalence point of the neutralization was reached and persisted through the end of the simulated neutralization. The modeling also indicated that >99.999% of the initial U added was precipitated in the form of sodium diuranate ( $\text{Na}_2\text{U}_2\text{O}_7$ ). In the case of the second simulant (Gd and Fe poisons), no sodium aluminosilicate phases were observed to form, and again >99.999% of the U in the system was present as  $\text{Na}_2\text{U}_2\text{O}_7$  at the end of the neutralization.

## TABLE OF CONTENTS

LIST OF TABLES .....	viii
LIST OF FIGURES .....	ix
LIST OF ABBREVIATIONS.....	x
1.0 Introduction.....	1
2.0 Experimental Procedure.....	1
2.1 Simulant Preparation .....	1
2.2 Neutralization Experiments.....	3
2.3 Physical Property Measurements .....	5
2.4 Sample Preparation for Rheological Measurements .....	6
2.5 Rheological Measurements .....	8
2.6 Flow Calculations.....	8
2.7 Critical Velocity and Sloped Piping .....	11
2.8 Literature Review and Modeling Regarding Formation of Aluminosilicates .....	15
2.9 Quality Assurance .....	16
3.0 Results and Discussion .....	16
3.1 Simulant Characterization .....	16
3.2 Neutralization Reactions .....	16
3.2.1 Simulant #1 .....	16
3.2.2 Simulant #2.....	19
3.3 Physical Property Measurements .....	21
3.3.1 As-Batched .....	21
3.3.2 Targeted Densities Results .....	24
3.4 Flow Calculations.....	27
3.5 Critical Velocity .....	30
3.6 Literature Review and Modeling Regarding Formation of Aluminosilicates .....	31
3.6.1 Literature Review .....	31
3.6.2 Summary of Literature Review Applied to Aluminosilicate Scale Formation during Neutralization .....	36
3.6.3 Results of GWB Modeling .....	38
4.0 Conclusions.....	39
5.0 Future Work.....	40
6.0 References.....	41
Appendix A . Elevation, Piping, and Fittings for H-Canyon Gravity Drain Lines to HPP 5 and HPP 6 A-1	

## LIST OF TABLES

Table 2-1. Expected Composition of an Average MTR Batch <sup>6</sup> .....	1
Table 2-2. Expected Composition of an Average HFIR Batch <sup>6</sup> .....	2
Table 2-3. Expected Compositions of Dissolver Solutions after Isotopic Adjustment.....	2
Table 2-4. Target Composition of Simulant #1 .....	3
Table 2-5. Target Composition of Simulant #2 .....	3
Table 2-6. Samples Collected During Neutralization Experiments .....	5
Table 2-7. Diluents for Particle Size Measurements.....	5
Table 2-8. Samples Prepared for Rheology Measurements .....	7
Table 2-9. Flow Curve Profile Using the MV1 Geometry.....	8
Table 2-10. Elevation drop, Pipe run, and fittings for 3” schedule 40 Waste Transfer Line Between Building 221-H to HPP#5 and HPP#6.....	11
Table 2-11. Crystal Densities of Precipitated Solids .....	13
Table 2-12. Basis Vectors for GWB Modeling.....	15
Table 3-1. Composition of Prepared Simulants .....	16
Table 3-2. Supernate Component Concentrations During Neutralization of Simulant #1.....	18
Table 3-3. Solid Component Concentrations During Neutralization of Simulant #1 .....	19
Table 3-4. Supernate Component Concentrations During Neutralization of Simulant #2.....	20
Table 3-5. Solid Component Concentrations During Neutralization of Simulant #2 .....	21
Table 3-6. Weight Percent Solids Concentrations and Densities of Endpoint Simulants.....	21
Table 3-7. Particle Size Distribution Data for Simulants #1 and #2 Endpoints.....	23
Table 3-8. Density and Weight Percent Total Solids of Dilutants.....	24
Table 3-9. Density, Wt% <sub>TS</sub> , Wt% <sub>IS</sub> , and Rheology Results for Simulant #1 Target Density Samples.....	25
Table 3-10. Density, Wt% <sub>TS</sub> , Wt% <sub>IS</sub> , and Rheology Results for Simulant #2, 0.6 M Target Density Samples .....	26
Table 3-11. Density, Wt% <sub>TS</sub> , Wt% <sub>IS</sub> , and Rheology Results for Simulant #2, 1.2 M Target Density Samples .....	27
Table 3-12. Flowrates for Simulant #1 .....	29
Table 3-13. Flowrates for Simulant #2, 0.6 M OH.....	29

Table 3-14. Flowrates for Simulant #2, 1.2 M OH.....	30
Table 3-15. Critical Velocity for Full Pipe Conditions.....	31
Table 3-16. Slope for 75 gpm and Average Pipeline and Critical Velocities for Average Slope.....	31

## LIST OF FIGURES

Figure 2-1. Photograph of jacketed reaction vessel and overhead mixer before being placed inside the radiological hood. ....	4
Figure 2-2. Disposition Froude Number for Small and Dense Particles (Ref. 20) .....	12
Figure 2-3. Partial Pipe Fill to Determine the Hydraulic Radius for a Given Fill Height .....	14
Figure 3-1. Photograph of solids collected on filter from Sample #2 during neutralization of Simulant #1. ....	17
Figure 3-2. Photograph of the reaction mixture at the point of maximum solids precipitation during neutralization of Simulant #1 (190 mL of 50 wt% NaOH had been added).....	18
Figure 3-3. Volumetric Particle Size Distribution for Simulant #1 Endpoints. ....	22
Figure 3-4. Volumetric Particle Size Distribution for Simulant #2 Endpoints. ....	23
Figure 3-5. Photograph of bottles containing product from each neutralization. From left to right: Simulant #1, 0.6 M OH <sup>-</sup> ; Simulant #1, 1.2 M OH <sup>-</sup> ; Simulant #2, 0.6 M OH <sup>-</sup> ; Simulant #2, 1.2 M OH <sup>-</sup> . ....	24
Figure 3-6. The mineral phases that were predicted by GWB 12.0.5 to precipitate during the neutralization of Simulant #1. ....	38
Figure 3-7. The mineral phases that were predicted by GWB 12.0.5 to precipitate during the neutralization of Simulant #2. ....	39

## LIST OF ABBREVIATIONS

ABD	Accelerated Basin De-inventory
ASNF	aluminum spent nuclear fuel
CSTF	Concentration, Storage, and Transfer Facility
DDI	distilled deionized
DU	depleted uranium
DWPF	Defense Waste Processing Facility
ELN	electronic laboratory notebook
GWB	Geochemist Workbench <sup>®</sup>
HFIR	High Flux Isotope Reactor
HLW	high level waste
HPP	H-Area Pump Pit
ICP-ES	inductively coupled plasma – emission spectroscopy
M&TE	Measuring and Test Equipment
MTR	Material Test Reactor
NCSE	Nuclear Criticality Safety Evaluation
ORNL	Oak Ridge National Laboratory
SaM	Sensing and Metrology
SME	Slurry Mix Evaporator
SRMC	Savannah River Mission Completion
SRNL	Savannah River National Laboratory
SRS	Savannah River Site
SRTC	Savannah River Technology Center
TTQAP	Task Technical and Quality Assurance Plan
TTR	Technical Task Request
XAFS	X-ray absorption fine structure
a	Variable used in Bingham Plastic turbulent friction factor
A	Cross-sectional area of flow
Ar	Archimedes Number
d <sub>50</sub>	50% tile particle diameter
D	Inside diameter of piping
f	Friction factor
F	Fill Factor
f <sub>L</sub>	Bingham Plastic friction factor
F <sub>L</sub>	Froude number from Wilson and Judge

$f_T$	Bingham Plastic turbulent friction factor
$g$	Gravitational acceleration
$K_f$	Entrance and exit losses
$L$	Length of piping
$\left(\frac{L}{D}\right)_{eq}$	Equivalent $\frac{L}{D}$ method for fittings
$m$	variable used to determine overall friction factor
$n$	Number of data points obtained at 600 sec <sup>-1</sup>
$N_{He}$	Hedstrom number
$N_{Re}$	Reynolds number
$N_{ReB}$	Bingham Reynolds number
$N_{ReB,C}$	Transitional Bingham Reynolds number
$P_w$	Wetted perimeter
$Q$	Volumetric flowrate
$R_H$	hydraulic radius
$T_C$	Cord Length
$V$	Average fluid velocity
$V_D$	Volume of diluent (0.6M or 1.2M excess NaOH)
$V_f$	Volume of starting slurry
$V_T$	Volume of target slurry
$wt\%_{DSS}$	Weight percent dissolved solids in the supernate
$wt\%_{IS}$	Weight percent insoluble solids in the slurry
$wt\%_{TS}$	Weight percent totals solids in slurry
$x_c$	critical value of the ratio of yield to wall stresses
$Y$	Fill height
$\Delta z$	Difference between inlet to outlet elevation
$\varepsilon$	Pipe roughness
$\dot{\gamma}$	Shear rate
$\theta$	Angle of fill
$\rho$	Fluid density
$\rho_D$	Density of diluent
$\rho_f$	Starting slurry density
$\rho_s$	Solids Density
$\rho_T$	Target slurry density
$\mu$	Viscosity
$\mu_\infty$	Bingham Plastic Viscosity

$\mu_{600\frac{1}{s}}$	Average apparent viscosity at $600 \text{ sec}^{-1}$
$\tau$	Measured shear stress
$\tau_o$	Bingham Plastic Yield Stress
$\left(\frac{\tau}{\dot{\gamma}}\right)_{600\frac{1}{s}}$	Apparent viscosity at $600 \text{ sec}^{-1}$
$\chi$	fraction of eddies with velocity

## 1.0 Introduction

Under the Accelerated Basin De-inventory (ABD) program H-Canyon will be dissolving aluminum spent nuclear fuel (ASNF) and then neutralizing that solution without performing head-end strike or uranium recovery operations.<sup>1</sup> The initial fuel to be dissolved under this program includes both High Flux Isotope Reactor (HFIR) and Material Test Reactor (MTR) fuel. The fuel will be dissolved in H-Canyon using the existing flowsheets,<sup>2,3</sup> which involve the addition of mercury (Hg) as a catalyst, gadolinium (Gd) as a neutron poison as needed, and nitric acid. After dissolution, the ABD material will be neutralized to a free hydroxide concentration of either 0.6 M or 1.2 M to meet the waste acceptance criteria<sup>4</sup> for transfer to the Concentration, Storage, and Transfer Facility (CSTF).

In order to ensure the material could be successfully neutralized and transferred to the CSTF, Savannah River National Laboratory (SRNL) conducted studies with a simulated H-Canyon dissolver solution. A bounding simulant was developed based on the expected compositions of HFIR and MTR fuels. Items to be addressed through the testing included determination if there was separation of the fissile and poison during the neutralization and if the rheology of the resultant slurry was such that it could be successfully transferred through the waste header to the CSTF. In addition, a literature survey was performed to determine if there are any concerns associated with the seeding of sodium aluminosilicates following the neutralization that could lead to the formation of scale on the wall of the tank which may also contain uranium.

## 2.0 Experimental Procedure

### 2.1 Simulant Preparation

The ABD program will include the dissolution of both MTR and HFIR fuels.<sup>5</sup> Information on the expected composition of batches of MTR and HFIR fuel<sup>6</sup> were used for evaluating potential simulant compositions in order to select a bounding composition for this work. The expected average composition of a batch of MTR fuel to be dissolved in the 6.1D dissolver is provided in Table 2-1. The HFIR fuel has a much higher level of <sup>235</sup>U enrichment, and therefore will require a larger dilution with depleted uranium to reach the ~ 3 or < 5 wt% <sup>235</sup>U target (as specified in the Technical Task Request (TTR))<sup>7</sup> for transfer to the CSTF, resulting in higher overall uranium concentrations. The expected composition of a batch of HFIR fuel consisting of 5 inner and 5 outer cores per batch in the 6.4D dissolver is provided in Table 2-2. The initial volumes of the 6.1D and 6.4D dissolvers are 7,500 L and 15,000 L, respectively. At the end of dissolution of a batch, the final volumes are expected to have decreased to 6,500 L and 13,875 L, respectively, due to evaporation (based on the average final volumes from recent dissolutions).<sup>8</sup>

**Table 2-1. Expected Composition of an Average MTR Batch<sup>6</sup>**

	Al	U	<sup>235</sup> U	Np	Pu	Si
<b>Mass per Batch (g)</b>	381,648	26,500	8,700	163	174	1400
<b>Concentration in Initial Dissolver Volume (g/L)</b>	50.9 (1.89 M)	3.53	1.16	0.022	0.023	0.19
<b>Concentration in Final Dissolver Volume (g/L)</b>	58.7 (2.18 M)	4.08	1.34	0.025	0.027	0.22

**Table 2-2. Expected Composition of an Average HFIR Batch<sup>6</sup>**

	Al	U	<sup>235</sup> U	Np	Pu
<b>Mass per Batch (g)</b>	664,881	39,787	34,276	58	70
<b>Concentration in Initial Dissolver Volume (g/L)</b>	44.3 (1.64 M)	2.65	2.29	0.0039	0.0047
<b>Concentration in Final Dissolver Volume (g/L)</b>	47.9 (1.78 M)	2.87	2.47	0.0042	0.0050

Compositions expected after adjustment of the <sup>235</sup>U enrichment to 3% and 5% as well as inclusion of the Gd poison at a mass ratio of 0.625 Gd:<sup>235</sup>U sludge equivalent (<sup>235</sup>U(eq<sub>SLU</sub>))<sup>a</sup> were calculated and are provided in Table 2-3, using the concentrations in the final dissolver solutions from Table 2-1 and Table 2-2 as input. An enrichment level of 0.15%, a total U concentration of 480 g/L, and an acid concentration of 0.25 M was used for the depleted uranium (DU) solution added for the isotopic adjustment.<sup>6</sup> Variations to the DU solution composition which may be more dilute or have higher acid concentrations are not expected to impact the outcome of this work. Higher acid concentrations will require additional sodium hydroxide addition during the neutralization, but would not be expected to impact the precipitation behavior. The minor components (i.e., Np, Pu, Si) were not included in these calculations, as their concentrations are not expected to significantly impact the results of the experiments planned. The values in Table 2-3 represent the final concentrations, using the expected final dissolver volumes<sup>8</sup> (accounting for evaporation during dissolution) and the depleted uranium addition.

**Table 2-3. Expected Compositions of Dissolver Solutions after Isotopic Adjustment**

	Al	U	<sup>235</sup> U	<sup>235</sup> U %	Gd
<b>HFIR Diluted to 5% <sup>235</sup>U (g/L)</b>	43.6	46.2	2.31	5.0	1.44
<b>HFIR Diluted to 3% <sup>235</sup>U (g/L)</b>	40.8	73.7	2.21	3.0	1.38
<b>MTR Diluted to 5% <sup>235</sup>U (g/L)</b>	56.0	26.2	1.31	5.0	0.82
<b>MTR Diluted to 3% <sup>235</sup>U (g/L)</b>	53.9	43.0	1.29	3.0	0.80

As seen from the values in Table 2-3, the HFIR solution diluted to 3% <sup>235</sup>U has the largest U concentration due to the higher enrichment level of this fuel. This composition is expected to be the most challenging in terms of rheology and flow due to the higher solids content, and therefore was selected as the bounding simulant for this work. Depleted uranium was used for all uranium in the simulant preparation as the isotopic composition will not affect the chemical (e.g., precipitation) behavior of the uranium. The expected acid concentration at the end of dissolution for both the HFIR and MTR flowsheets is predicted to be about 1.5 M HNO<sub>3</sub>. The target simulant composition is provided in Table 2-4, taking into account the dilution following the addition of the DU solution.<sup>6</sup>

<sup>a</sup> The 0.625 Gd:<sup>235</sup>U(eq<sub>SLU</sub>) was specified in the TTR; however, different facilities may utilize different <sup>235</sup>U equivalent formulas depending on what is applicable to a given facility.

**Table 2-4. Target Composition of Simulant #1**

Component	Concentration in Simulant
Al	40.8 g/L
U	73.7 g/L
Gd	1.38 g/L
HNO <sub>3</sub>	1.31 M

In order for the Liquid Waste Contractor, Savannah River Mission Completion (SRMC), to authorize the addition of ABD material to Sludge Batch 11, it is likely that SRMC may require the addition of iron as a poison prior to the transfer. As adding iron will increase the solids content of the neutralized stream, and therefore impact the rheology, an additional simulant was also prepared adding iron at a 160:1 Fe:<sup>239</sup>Pu equivalent ratio.<sup>9</sup> The <sup>239</sup>Pu equivalence is defined below in equations 1 and 2.<sup>9</sup> The composition of the simulant to be prepared with iron is provided in Table 2-5. The facility would add iron as a 41 wt% solution of iron nitrate (135 g/L Fe).

$$^{239}\text{Pu}(\text{eq}) = ^{239}\text{Pu} + ^{241}\text{Pu} + ^{244}\text{Cm} + 15(^{245}\text{Cm}) + 35(^{242\text{m}}\text{Am}) + 0.65(^{235}\text{U}(\text{eq}_{\text{SLU}})) \quad (1)$$

$$^{235}\text{U}(\text{eq}_{\text{SLU}}) = ^{235}\text{U} + 1.4(^{233}\text{U}) \quad (2)$$

**Table 2-5. Target Composition of Simulant #2**

Component	Concentration in Simulant
Al	15.1 g/L
U	27.3 g/L
Gd	0.51 g/L
Fe	85.1 g/L
HNO <sub>3</sub>	0.49 M

The uranium used for preparing both simulants was obtained through dissolution of a sample of U<sub>3</sub>O<sub>8</sub> containing depleted uranium. For Simulant #1, the U<sub>3</sub>O<sub>8</sub> was dissolved in nitric acid to a target concentration of 150 g/L with a final nitric acid concentration of 1.5 M. Analysis of the product from dissolution indicated the solution was 143 g/L U and had a nitric acid concentration of 1.78 M. The simulant was prepared by dissolving 2.41 g of gadolinium nitrate hexahydrate and 344.33 g of aluminum nitrate nonahydrate in distilled deionized (DDI) water. 15.16 mL of concentrated nitric acid and 313 mL of the DU solution were then added to give a final volume of 612 mL. A sample of the prepared simulant was analyzed by inductively coupled plasma – emission spectroscopy (ICP-ES) and free acid titration to confirm the metal and nitric acid concentrations.

For Simulant #2, the U<sub>3</sub>O<sub>8</sub> was again dissolved in nitric acid, this time to a target concentration of 100 g/L U and a final nitric acid concentration of 1.6 M. Analysis of the product from dissolution indicated the solution was 97.9 g/L U and had a nitric acid concentration of 1.90 M. Simulant #2 was then prepared by dissolving 0.9015 g of gadolinium nitrate hexahydrate, 128.87 g of aluminum nitrate nonahydrate, and 377.79 g of ferric nitrate nonahydrate in DDI water. 171 mL of the DU solution was then added to give a final volume of 614 mL. A sample of the prepared simulant was analyzed by ICP-ES and free acid titration to confirm the metal and acid concentrations.

## 2.2 Neutralization Experiments

Neutralization of each simulant was performed by the addition of 50 wt% (18.9 M) sodium hydroxide solution to the starting simulant while mixing with an overhead mixer and Rushton impeller. The reactor

vessel had no baffles, and the impeller was installed at an angle to provide better mixing. For Simulant #1 the starting volume was 608 mL and for Simulant #2 the starting volume was 610 mL. Figure 2-1 is that of the vessel and mixer used for neutralizations. The vessel included a water jacket for cooling of the mixture during neutralization to ensure the temperature remained below 60 °C. The temperature was monitored throughout the neutralization with a Measuring and Test Equipment (M&TE) calibrated thermocouple. The sodium hydroxide was added at a controlled rate through the use of a syringe pump. A 60-mL syringe was loaded with 50 wt% NaOH solution, and tubing was used to deliver NaOH from the syringe to the reaction vessel at an addition rate between 2 to 4 mL/min. The impeller speed was adjusted throughout the NaOH addition to maintain a slight vortex in the vessel. The impeller speed ranged from 250 rpm at the start of the addition to 1100 rpm at the point in the addition where mixing became most difficult. Samples were removed periodically throughout the neutralization reaction. The solid and liquid phases from each sample collected were separated either through filtration or in some cases centrifugation. Liquid phase samples were diluted with deionized water prior to submitting for analysis. Solid samples were dissolved in either 8 M or concentrated (15.7 M) HNO<sub>3</sub> and then diluted with water prior to analysis. A summary of samples taken and analyses performed is provided in Table 2-6. The 50 wt% NaOH addition proceeded until reaching the calculated quantity of NaOH required to reach an end point of 0.6 M free hydroxide. At this point the slurry was transferred from the reaction vessel and roughly equal amounts were placed in two separate polyethylene bottles. During the transfer the volume placed into each bottle was measured. The calculated quantity of 50 wt% NaOH necessary to reach 1.2 M free hydroxide was added to one of the bottles and was mixed by manual shaking of the bottle. These two bottles at 0.6 M and 1.2 M free hydroxide were then used for further physical property measurements and flow calculations described in the next section.



**Figure 2-1. Photograph of jacketed reaction vessel and overhead mixer before being placed inside the radiological hood.**

**Table 2-6. Samples Collected During Neutralization Experiments**

Simulant #1			
Sample #	Volume of 50 wt% NaOH added	pH	Analyses
1	55 mL	< 2	Filtrate and digested solids: ICP-ES
2	100 mL	~2.5	Filtrate and digested solids: ICP-ES
3 <sup>a</sup>	195 mL	NM <sup>b</sup>	Digested solids: ICP-ES
4	291.4 mL	NM, 0.6 M free OH (calculated)	Filtrate and digested solids: ICP-ES; slurry: particle size and weight percent solids: density
5	321.4 mL <sup>c</sup>	NM, 1.2 M free OH (calculated)	Filtrate and digested solids: ICP-ES; slurry: particle size and weight percent solids: density
Simulant #2			
Sample #	Volume of 50 wt% NaOH added	pH	Analyses
1	50 mL	< 2	Filtrate and digested solids: ICP-ES
2	150 mL	< 2	Filtrate and digested solids: ICP-ES
3 <sup>d</sup>	225 mL	NM	Filtrate and digested solids: ICP-ES
4	270 mL	NM, 0.6 M free OH (calculated)	Filtrate and digested solids: ICP-ES; slurry: particle size and weight percent solids: density
5	295.8 mL <sup>c</sup>	NM, 1.2 M free OH (calculated)	Filtrate and digested solids: ICP-ES; slurry: particle size and weight percent solids: density

<sup>a</sup> Mixture was nearly solid at this point of the neutralization. Difficult to obtain good mixing and unable to collect a liquid sample. A sample of the solid was collected using a spatula. <sup>b</sup> NM = not measured. <sup>c</sup> This is equivalent to the amount added if the sample was not split at the 0.6 M end point as described above. <sup>d</sup> Mixture very viscous at this point of the neutralization with a large quantity of precipitated solids. A small amount of filtrate was obtained for analysis.

### 2.3 Physical Property Measurements

Samples from each of the end points (0.6 M and 1.2 M free hydroxide) were submitted to Sensing and Metrology (SaM) for particle size and weight percent solids analysis. Particle size measurements were performed using a Microtrac S3500 instrument. Samples of the slurry were submitted for analysis along with a diluent prepared to match the major composition of the supernate. This diluent was used to dilute samples of the slurry in the instrument for particle size measurements. Compositions of the diluents prepared are provided in Table 2-7. Weight percent solids measurements were completed in triplicate for each sample. A sample of the slurry (approximately 3 g) was placed into a glass beaker and dried in an oven at 115 °C until a constant weight was achieved to obtain the weight percent total solids (wt%<sub>TS</sub>). In addition, a sample of the slurry was filtered through a 0.2-μm filter to obtain a sample of filtrate. The filtrate sample was also placed into a beaker and dried at 115 °C until a constant weight was achieved to obtain the weight percent of dissolved solids in the supernate (wt%<sub>DSS</sub>). Finally, the weight percent insoluble solids (wt%<sub>IS</sub>) was calculated using equation (3).

**Table 2-7. Diluents for Particle Size Measurements**

Component	Concentration (M)			
	Simulant #1 0.6 M Free OH endpoint	Simulant #1 1.2 M Free OH endpoint	Simulant #2 0.6 M Free OH endpoint	Simulant #2 1.2 M Free OH endpoint
Al(NO <sub>3</sub> ) <sub>3</sub> ·9H <sub>2</sub> O	0.997	0.958	0.365	0.343
NaOH	4.59 (0.60 M free)	5.03 (1.2 M free)	2.06 (0.60 M free)	2.57 (1.2 M free)
NaNO <sub>3</sub>	1.40	1.91	3.75	3.48

$$\text{wt}\%_{\text{IS}} = \frac{\text{wt}\%_{\text{TS}} - \text{wt}\%_{\text{DSS}}}{100\% - \text{wt}\%_{\text{DSS}}} \cdot 100\% \quad (3)$$

Where:  $\text{wt}\%_{\text{TS}}$  = weight percent totals solids in slurry  
 $\text{wt}\%_{\text{DSS}}$  = weight percent dissolved solids in the supernate  
 $\text{wt}\%_{\text{IS}}$  = weight percent insoluble solids in the slurry

The densities of the resulting slurries obtained at the 0.6 M and 1.2 M free hydroxide end points were measured using a M&TE density meter (Storage Battery Systems, SBS 3500 digital hydrometer).

## 2.4 Sample Preparation for Rheological Measurements

Given the 1.35 g/mL density limit for neutralized slurries in H-Canyon,<sup>10</sup> the 0.6 M and 1.2 M free hydroxide slurries from both neutralizations were diluted with additional 0.6 M and 1.2 M NaOH solution to bring the density down to 1.35 g/mL and other targeted densities below this value. The 0.6 and 1.2 M NaOH solutions were prepared using 50 wt% NaOH solution and DDI water, volumetrically. The densities of the 0.6 and 1.2 M NaOH solutions were obtained from reference<sup>11</sup> given the molarities.

Duplicate rheological measurements require a total of 75 mL of slurry. To determine the volumes of the starting slurries (endpoint simulant) and diluents (0.6 and 1.2 M NaOH), volume additivity<sup>12</sup> was used. Equations (4) and (5) were used to determine volume additions for the diluent and starting slurry, respectively. A summary of targeted slurry samples prepared for rheology measurements is provided in Table 2-8, given the batched densities of the starting simulants.

$$V_D = \frac{(\rho_T - \rho_f)}{(\rho_D - \rho_f)} \cdot V_T \quad (4)$$

$$V_f = V_T - V_D \quad (5)$$

Where:  $V_D$  = volume of diluent (0.6 or 1.2 M NaOH)  
 $V_f$  = volume of starting slurry  
 $V_T$  = volume of target slurry  
 $\rho_T$  = target slurry density  
 $\rho_f$  = starting slurry density  
 $\rho_D$  = density of diluent

**Table 2-8. Samples Prepared for Rheology Measurements**

<b>Simulant #1 0.6 M Free Hydroxide</b>		
<b>Target Density (g/mL)</b>	<b>Volume of Feed (mL)</b>	<b>Volume of 0.6 M NaOH (mL)</b>
1.35	69.2	5.8
1.33	64.9	10.1
1.31	60.7	14.3
1.27	52.1	22.9
<b>Simulant #1 1.2 M Free Hydroxide</b>		
<b>Target Density (g/mL)</b>	<b>Volume of Feed (mL)</b>	<b>Volume of 1.2 M NaOH (mL)</b>
1.35	67.3	7.7
1.33	62.8	12.2
1.31	58.3	16.7
1.27	49.3	25.7
<b>Simulant #2 0.6 M Free Hydroxide</b>		
<b>Target Density (g/mL)</b>	<b>Volume of Feed (mL)</b>	<b>Volume of 0.6 M NaOH (mL)</b>
1.35	71.1	3.9
1.33	66.7	8.3
1.31	62.3	12.7
1.29	57.9	17.1
1.25	49.2	25.8
1.21	42.7 <sup>a</sup>	32.3
<b>Simulant #2 1.2 M Free Hydroxide</b>		
<b>Target Density (g/mL)</b>	<b>Volume of Feed (mL)</b>	<b>Volume of 1.2 M NaOH (mL)</b>
1.35	69.6	5.4
1.33	65.0	10.0
1.31	60.3	14.7
1.29	55.7	19.3
1.25	46.4	28.6
1.21	40.1 <sup>a</sup>	34.9

<sup>a</sup> Prepared using the 1.35 g/mL sample, volume reflects volume of 1.35 g/mL slurry versus original feed.

The densities of the 0.6 M and 1.2 M NaOH solutions and the target density samples in Table 2-8 above were measured after the rheological measurements were completed. The wt%DSS in the 0.6 M and 1.2 M NaOH solutions were obtained from reference 11. The wt%<sub>IS</sub> and wt%<sub>TS</sub> for the target density samples were calculated using equations (6) and (7), respectively.

$$\text{wt}\%_{\text{IS},\text{sample}} = \frac{\text{wt}\%_{\text{IS},f} \cdot V_f \cdot \rho_f}{(V_f + V_D) \cdot \rho_{\text{sample}}} \quad (6)$$

$$\text{wt}\%_{\text{TS},\text{sample}} = \frac{\text{wt}\%_{\text{TS},f} \cdot V_f \cdot \rho_f + \text{wt}\%_{\text{TS},D} \cdot V_D \cdot \rho_D}{(V_f + V_D) \cdot \rho_{\text{sample}}} \quad (7)$$

Where: wt%<sub>IS,sample</sub> = weight percent of insoluble solids after dilution  
 wt%<sub>TS,sample</sub> = weight percent of total solids dilution  
 wt%<sub>IS,f</sub> = weight percent of insoluble solids as batched slurry  
 wt%<sub>TS,f</sub> = weight percent of total solids of as batched slurry  
 wt%<sub>TS,D</sub> = weight percent of dissolved solids of as dilution  
 ρ<sub>sample</sub> = target sample density

## 2.5 Rheological Measurements

Flow curves (shear stress versus shear rate) were obtained using a Haake VT550 roto-viscometer. Initial setup included determining the water bath temperature that would yield viscosity of three NIST traceable oil standards as specified on the certificate of analyses at 25 °C, to within +/- 3% of the published value, this resulted in setting the bath water temperature to 26 °C for subsequent measurements. The VT550 was then functional checked using a NIST traceable oil standard the day flow curve measurements were obtained. Samples were prepared by shaking the bottle, swirling to assist in removing entrained air, loading into the cup, raising into heating/cooling bath jacket, trimming excess fluid, zeroing the torque on the VT550 manually, and starting the measurement using the sludge flow curve profile shown in Table 2-9. Sufficient volume for each sample condition was made to allow for two independent measurements and the rheological results were averaged.

**Table 2-9. Flow Curve Profile Using the MV1 Geometry**

Up Curve	Hold	Down Curve	Sample Volume
0 to 600 s <sup>-1</sup> linearly in 5 min	600 s <sup>-1</sup> for 1 min	600 to 0 s <sup>-1</sup> linearly in 5 min	35 mL

The resulting up and down curves were fitted to Bingham Plastic rheological model, equation (8).

$$\tau = \tau_o + \mu_{\infty} \cdot \dot{\gamma} \quad (8)$$

Where:  $\tau$  = measured shear stress

$\tau_o$  = Bingham Plastic Yield Stress

$\mu_{\infty}$  = Bingham Plastic Viscosity

$\dot{\gamma}$  = shear rate

The average apparent viscosity (equation (9)) at the maximum shear rate (600 s<sup>-1</sup>) is obtained and will be used if the fluid is analyzed as a Newtonian fluid.

$$\mu_{600 \frac{1}{s}} = \frac{\sum_n \left( \frac{\tau}{\dot{\gamma}} \right)_{600 \frac{1}{s}}}{n} \quad (9)$$

Where:  $\mu_{600 \frac{1}{s}}$  = average apparent viscosity at 600 sec<sup>-1</sup>

$\left( \frac{\tau}{\dot{\gamma}} \right)_{600 \frac{1}{s}}$  = apparent viscosity at 600 sec<sup>-1</sup>

n = number of data points obtained at 600 sec<sup>-1</sup>

## 2.6 Flow Calculations

In this case, only full pipe analysis was performed. This provides an ideal of the maximum flow that could be obtained and if the actual flowrates feeding the gravity feed lines are higher, the material will back-up in the 10-inch header. For flowrates lower than this, the pipe will be partially filled and calculations can be performed to determine fill height and average velocity if necessary.

The calculations are based on the method Darby presents in reference 13. It is assumed that the vapor pressure in the 10-inch header and the receipt vessel are essentially the same, hence the change in elevation will equate to the frictional losses due to piping and fittings. This is shown as equation (10) and is derived from equations (6-2), (6-5) and (7-34)<sup>13</sup>.

$$g\Delta z = \frac{4L}{D} f \frac{V^2}{2} + 4f \frac{V^2}{2} \sum \left( \frac{L}{D} \right)_{eq} + \frac{V^2}{2} \sum K_f \quad (10)$$

Where:  $\Delta z$  = difference between inlet to outlet elevation

$g$  = gravitational acceleration

$V$  = Average fluid velocity

$L$  = length of piping

$D$  = inside diameter of piping

$f$  = friction factor

$\left(\frac{L}{D}\right)_{eq}$  = equivalent  $\frac{L}{D}$  method for fittings

$K_f$  = entrance and exit losses

The  $\left(\frac{L}{D}\right)_{eq}$  for the fittings were obtained from Crane.<sup>14</sup> Crane states turbulent friction factors as denoted in their manual should be used, but in this case, the friction factor is calculated using equation (11). This results in a higher pressure drop, hence is conservative.

For Newtonian fluids, the friction factor is determined using Colebrook's equation, equation (11).<sup>13</sup> This equation is applicable for turbulent flow,  $N_{Re} > 4000$ . Clean pipe and rusty pipe flow calculations will be performed. For clean pipe,  $\varepsilon = 0.00015$  ft and for light and general rust  $\varepsilon = 0.00125$  ft and 0.00667 ft, respectively.<sup>15</sup>

$$\frac{1}{\sqrt{f}} = -4 \cdot \log \left[ \frac{\varepsilon}{3.7 \cdot D} + \frac{1.255}{N_{Re} \sqrt{f}} \right] \quad (11)$$

Where:  $\varepsilon$  = pipe roughness

$N_{Re} = \frac{\rho V D}{\mu}$  = Reynolds number

$\rho$  = fluid density

$\mu$  = viscosity

For Bingham Plastic fluids, equations (12) through (16) will be used. These equations are independent of pipe roughness, hence are for smooth pipe analysis. Note roughness does not impact laminar flow analysis.

$$f_L = \frac{16}{N_{ReB}} \left[ 1 + \frac{1}{6} \frac{N_{He}}{N_{ReB}} - \frac{1}{3} \frac{N_{He}^4}{f^3 N_{ReB}^7} \right] \quad (12)$$

$$f_T = \frac{10^a}{N_{ReB}^{0.193}} \quad (13)$$

$$a = -1.47 \cdot [1 + 0.146 \cdot e^{-2.9 \times 10^{-5} N_{He}}] \quad (14)$$

$$f = (f_L^m + f_T^m)^{\frac{1}{m}} \quad (15)$$

$$m = 1.7 + \frac{40000}{N_{ReB}} \quad (16)$$

Where:  $f_L$  = Bingham Plastic friction factor

$f_T$  = Bingham Plastic turbulent friction factor

$a$  = variable used in Bingham Plastic turbulent friction factor

$m$  = variable used to determine overall friction factor

$N_{ReB} = \frac{\rho V D}{\mu_\infty}$  = Bingham Reynolds number

$N_{He} = \frac{D^2 \cdot \rho \cdot \tau_0}{\mu_\infty^2}$  = Hedstrom number

To estimate the transition from laminar to turbulent for Bingham Plastic fluids, the method proposed by Hanks<sup>16</sup>, equations (17) and (18) will be used. This is applicable for  $10^4 < N_{ReB} < 10^7$ .<sup>17</sup>

$$N_{ReB,C} = \frac{N_{ReB}}{8 \cdot x_c} \left( 1 - \frac{4}{3} x_c + \frac{1}{3} x_c^4 \right) \quad (17)$$

$$\frac{x_c}{(1 - x_c)^3} = \frac{N_{ReB}}{16,800} \quad (18)$$

Where:  $N_{ReB,C}$  = Transitional Bingham Reynolds number

$x_c$  = critical value of the ratio of yield to wall stresses

The flowrate is calculated using equation (19).

$$Q = \pi \cdot V \cdot \left( \frac{D}{2} \right)^2 \quad (19)$$

Where:  $Q$  = volumetric flowrate

The elevation drop, pipe runs, and fittings from Building 221-H to H-Area Pump Pit (HPP)#5 and HPP#6 are based on drawings W715433, W712040, W712649, W712042, W712648, W714352, W714341, W713240, W716075, W716076, and W716212 and are shown in Appendix A. The various drain lines are colored blue, green, yellow, and pink for transfer lines WF1100, WF1101, WF1102, and WF1103, respectively. WF1103 information is provided, but this line is not in service. WF1100 and W1102 will be used in this analysis and bound WF1101. Table 2-10 provides a summary of the hydraulic systems for the four different discharge lines leaving 221-H to the HPP. Table 2-10 contains the elevation drop, piping run,  $K$ , and the number and total  $\left( \frac{L}{D} \right)_{eq}$  for each elbow of having a radius bend to pipe diameter ratios as provided in the drawings.

**Table 2-10. Elevation drop, Pipe run, and fittings for 3” schedule 40 Waste Transfer Line Between Building 221-H to HPP#5 and HPP#6**

	WF1100		WF1101		WF1102		WF1103	
$\Delta H$	19.03 ft		17.22 ft		15.81 ft		14.73 ft	
Pipe Run	756.9 ft		770.6 ft		775.0 ft		752.6 ft	
	Number	K	Number	K	Number	K	Number	K
Entrance	1	0.5	1	0.5	1	0.5	1	0.5
Exit	1	1	1	1	1	1	0	0
Elbow (r/d)	Number	$\left(\frac{L}{D}\right)_{eq}$	Number	$\left(\frac{L}{D}\right)_{eq}$	Number	$\left(\frac{L}{D}\right)_{eq}$	Number	$\left(\frac{L}{D}\right)_{eq}$
1	1	20	1	20	1	20	1	20
1.5	5	70	5	70	4	70	5	70
2	0	0	1	12	1	12	0	0
5	2	32	2	32	2	32	1	16
7	3	63	3	63	3	63	3	63
90° Mitre	2	120	2	120	2	120	2	120
$\left(\frac{L}{D}\right)_{eq,total}$		305		317		303		289

## 2.7 Critical Velocity and Sloped Piping

The critical velocity is the velocity at which solids will deposit (settle) to the bottom of the pipeline to form a bed at the bottom of the pipe from fully suspended flow.<sup>18</sup> The critical velocity is determined from the physical properties of the solids being transported and of the carrier fluid, and the inside diameter of the pipe. The results for such testing resulted in correlations that are fitted to physics or non-physics based phenomena. Other correlations have been developed to cover a broad range of solids, fluids, and pipe sizes, such as those developed by Wasp's<sup>19</sup> and Oroskar and Turian<sup>18</sup>, equations (20) and (21) respectively. Their correlations also took into consideration the solids concentration. Typically, these correlations are based on commercial applications, where the mean (50 vol. % tile) particle size is around 100 to 200 microns, outside the range of interest for this work.

Given the particle of interest is dense and small (5 to 15 microns), the correlation developed and discussed by Poloski<sup>20</sup> will be utilized as well as an upper limit developed by Wilson and Judge as described in Poloski's article for such particles. Poloski's method (equations (22) through (24)) is applicable for Archimedes (Ar) numbers less than 80 and the Wilson and Judge results are shown in Figure 2-2 and used with equation (24). The Wilson and Judge Froude (Fr) number will be determined based on the calculated Ar number. The pipe diameter has been replaced with the hydraulic radius, to provide an indication of how the critical velocity and pipe velocity are impacted by sloped piping. The viscosity of the slurries will be based on the Newtonian viscosities at the measured maximum shear rate of  $600 \frac{1}{sec}$ .

$$V_d = 3.116 \cdot C_V^{0.186} \cdot \left(\frac{d_{50}}{4 \cdot R_H}\right)^{\frac{1}{6}} \cdot \left(8 \cdot g \cdot R_H \cdot \left(\frac{\rho_s}{\rho} - 1\right)\right)^{0.50} \quad (20)$$

$$V_d = 1.85 \cdot C_v^{0.1536} \cdot (1 - C_v)^{0.3564} \cdot \left( \frac{d_{50}}{4 \cdot R_H} \right)^{-0.378} \cdot \sqrt{g \cdot d_{50} \cdot \left( \frac{\rho_s}{\rho} - 1 \right)} \cdot \left( \frac{4 \cdot R_H \cdot \rho_l \cdot \sqrt{g \cdot d_{50} \cdot \left( \frac{\rho_s}{\rho} - 1 \right)}}{\mu} \right)^{0.09} \cdot (\chi)^{0.30} \quad (21)$$

$$Ar = \frac{4}{3} \cdot \frac{g \cdot d_{50}^3 \cdot \left( \frac{\rho_s}{\rho} - 1 \right) \cdot \rho^2}{\mu^2} \quad (22)$$

$$Fr = 0.59 Ar^{0.15} \quad (23)$$

$$V_d = Fr \cdot \left( 4 \cdot g \cdot R_H \cdot \left( \frac{\rho_s}{\rho} - 1 \right) \right)^{0.50} \quad (24)$$

Where:  $V_d$  = critical velocity

$C_v$  = volumetric concentration of solids

$d_{50}$  = 50% tile particle diameter

$R_H$  = hydraulic radius

$\rho_s$  = solids density

$\chi$  = fraction of eddies with velocity =  $0.96^{19}$

$Fr$  = Froude number from Wilson and Judge in Figure 2-2 or Poloski (equation (23))

$Ar$  = Archimedes Number

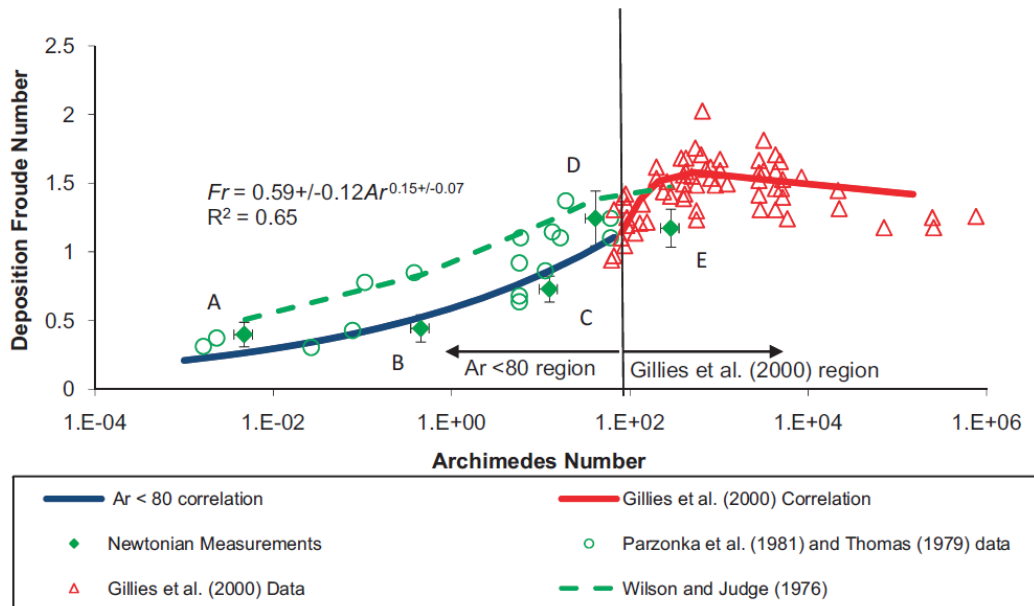


**Figure 2-2. Disposition Froude Number for Small and Dense Particles (Ref. 20)**

The average pipeline velocity should have a margin 30% greater than the largest critical velocity for conservatism.<sup>21</sup>

The precipitated solids of the simulants generated in this task are assumed to be of the forms stated in Table 2-11. The crystal particle densities of the solids and the reference where the data was obtained is provided. The solids generated during the precipitation process are flocculated, where the voided volume is filled with supernate. The crystal particle densities are greater than the flocculated densities,<sup>22</sup> hence the use of crystal density is conservative. For example, if the  $\text{Na}_2\text{U}_2\text{O}_7$  floc contained 20 vol. % of 1.35 g/mL supernate, the density of the floc would be 5.53 g/mL rather than the crystal density of 6.57 g/mL. Given the same particle size distribution would be used for any solids species, the uranium species, given it has the largest crystal density, will have the largest Ar number, resulting in the highest critical velocity and will be used in the analysis.

**Table 2-11. Crystal Densities of Precipitated Solids**

Solids	Density (g/mL)	Reference
$\text{NaAl}(\text{OH})_4$	1.34	T. P. Kropyvnytska and et al., “The effect of sodium aluminate on the properties of composite cements”, IOP Conference Series – Materials Science and Engineering, 2019
$\text{Fe}(\text{OH})_3$	3.4	<a href="http://www.aqua-calc.com/page/density-table/substance/ferric-blank-hydroxide">www.aqua-calc.com/page/density-table/substance/ferric-blank-hydroxide</a>
$\text{Na}_2\text{U}_2\text{O}_7$	6.57	A.L Smith and et al., “Thermodynamic investigation of $\text{Na}_2\text{U}_2\text{O}_7$ using Knudsen effusion mass spectrometry and high temperature X-ray Diffraction”, Vol. 90, pp. 199-208, Journal Chemical Thermodynamics, 2015
$\text{Gd}(\text{OH})_3$	5.6	A.J. Tan and et al., “Hydration of Gadolinium oxide ( $\text{GdO}_x$ ) and its effect on voltage-induced Co oxidation in a Pt/Co/ $\text{GdO}_x$ /Au heterostructure”, Vol. 3, Physical Review Materials, 2019

The average velocity and hydraulic radius will be determined for sloped piping. The sloped piping is assumed to be at steady state without any fitting or entrance losses. Calculations will be performed using pipe roughness of 0.00015 ft. EXCEL’s goal seek function is used to determine:

- Slope required to obtain full pipe conditions at 75 gpm
- The average velocity at 75 gpm and the critical velocity for the average slope of line 1100.

For line 1100, the slope of the pipe ranges from 0.00503 to 0.32645  $\text{ft}_{\text{vertical}}/\text{ft}_{\text{horizontal}}$ . Of the approximately 767 feet of sloped pipe run, 534 feet has a slope of 0.01553  $\text{ft}_{\text{vertical}}/\text{ft}_{\text{horizontal}}$ . The piping as it leaves the facility is steep and as sections of piping are added, the average slope ranges from 0.32645 (at the start) to 0.02194 (near the discharge), with an overall average of 0.02232  $\text{ft}_{\text{vertical}}/\text{ft}_{\text{horizontal}}$ . This average value will be used to determine the average pipeline velocity and critical velocities. See Appendix A for the piping runs.

For any given sloped line, excluding fitting or exit/entry losses, equation (10) becomes equation (25)

$$\frac{\Delta z}{L} = \frac{4}{g \cdot D} f \frac{V^2}{2} \quad (25)$$

The friction factor for partially full pipe is equation (26).<sup>23</sup> This is the Fanning friction factor, equation (25) is based on the Darcy friction factor, hence  $f = 4f_f$ .

$$\frac{1}{\sqrt{f_f}} = -2 \cdot \log \left( \frac{\varepsilon}{12 \cdot R_H} + \frac{2.51}{N_{Re,f} \sqrt{f_f}} \right), \text{ where } N_{Re,f} = \frac{4 \cdot \rho \cdot V \cdot R_H}{\mu} \quad (26)$$

Substituting the hydraulic radius for  $D$  and the Fanning friction factor, equation (25) becomes equation (27), which will be solved.

$$\frac{\Delta z}{L} = \frac{f_f}{4 \cdot g \cdot R_H} \frac{V^2}{2} = \frac{f_f \cdot V^2}{8 \cdot g \cdot R_H} \quad (27)$$

The velocity and hydraulic radius for a partially filled pipe can be determined using geometry as shown in Figure 2-3. Figure 2-3 shows the cross sectional of a partially filled pipe.

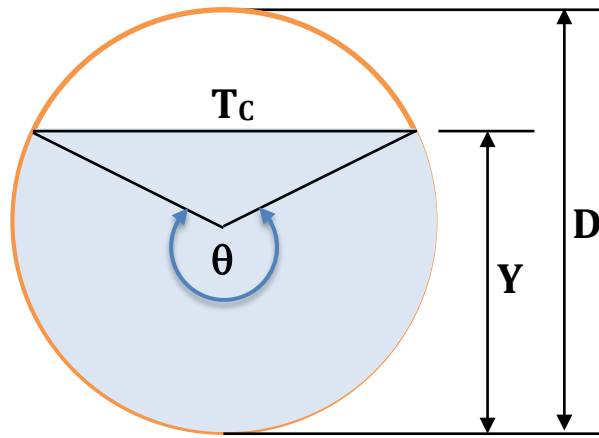


**Figure 2-3. Partial Pipe Fill to Determine the Hydraulic Radius for a Given Fill Height**

Where:

$Y$  = fill height

$F$  = fill factor =  $\frac{Y}{D}$

$\theta$  = angle of fill =  $2 \cdot \arccos(1 - 2 \cdot F)$

$T_c$  = chord length =  $D \sin\left(\frac{\theta}{2}\right)$

$A$  = cross-sectional area of flow =  $\frac{D^2 \cdot (\theta - \sin\theta)}{8}$

$P_w$  = wetted perimeter =  $\frac{D \cdot \theta}{2}$

The hydraulic radius is the ratio of the cross-sectional area of flow divided by the wetted perimeter, equation (28). Given the cross-section area of flow, the average velocity is determined using equation (29).

$$R_H = \frac{A}{P_w} = \frac{\frac{D^2 \cdot (\theta - \sin\theta)}{8}}{\frac{D \cdot \theta}{2}} = \frac{D \cdot (\theta - \sin\theta)}{4 \cdot \theta} \quad (28)$$

$$V = \frac{Q}{A} = \frac{8 \cdot Q}{D^2 \cdot (\theta - \sin\theta)} \quad (29)$$

The critical velocity will be calculated using the hydraulic radius of the average sloped pipe and this value will be compared to the velocity of the sloped pipe calculations.

## 2.8 Literature Review and Modeling Regarding Formation of Aluminosilicates

A literature survey was conducted to determine the feasibility of forming sodium aluminosilicates following the neutralization of the ASNF which could result in the formation of scale on the wall of the tank which may also contain U. The literature survey uncovered previous work where modeling was performed using a commercially available software package, The Geochemist Workbench® (GWB). Similar modeling was then performed using the expected composition of the neutralized streams studied in this work (starting with 1 L of simulant prior to neutralization). Si was not included in the experimental simulant work; however, was added to the modeling due to the need for Si to form potential aluminosilicates. The amount of Si was based upon a bounding amount determined in prior work.<sup>24</sup> Modeling was performed using the REACT module of the GWB in conjunction with the Yucca Mountain Project (YMP) thermodynamic dataset. This database invokes the Harvie-Møller-Weare activity formalism of the Pitzer equations, which allows high ionic strength solutions to be modeled using virial activity coefficients for solution species. The solution compositions were used to establish the two input basis vectors for the calculations – the basis vectors are given in Table 2-12.

**Table 2-12. Basis Vectors for GWB Modeling**

Simulant #1		Simulant #2	
Input Species	Moles	Input Species	Moles
Al <sup>+++</sup> (as Al)	1.4751	Al <sup>+++</sup> (as Al)	0.5263
UO <sub>2</sub> <sup>++</sup> (as U)	0.3201	UO <sub>2</sub> <sup>++</sup> (as U)	0.1092
Gd <sup>+++</sup> (as Gd)	0.00897	Gd <sup>+++</sup> (as Gd)	0.0032
NO <sub>3</sub> <sup>-</sup>	6.21241	Fe <sup>++</sup> (as Fe)	1.5221
SiO <sub>2</sub> (aq)	0.0067	NO <sub>3</sub> <sup>-</sup>	6.7742
Na <sup>+</sup>	1.0e-23	SiO <sub>2</sub> (aq)	0.0067
H <sup>+</sup> (as pH)	balance	Na <sup>+</sup>	1.0e-23
H <sub>2</sub> O	1.258 (kg)	H <sup>+</sup> (as pH)	balance
		H <sub>2</sub> O	1.202 (kg)

The total amount of nitrate was determined by considering the addition of the metal cations as nitrates to the original solution. The amounts of starting nitrate and metals were based on 1 L of the starting simulant. The concentration of the hydrogen ion was used to charge balance the solutions and the initial amount of water was adjusted such that the final solution volume (at the end of the modeled neutralization) was equivalent to that measured during the neutralization experiments. Sodium was included in the basis vector to allow for its addition as a reactant.

The neutralization was modeled by concurrently adding 9.8304 mol of Na<sup>+</sup> and 9.8304 mol of OH<sup>-</sup> to the basis vector in steps of 0.0983 mol/step for Simulant #1 and 9.1921 mol of Na<sup>+</sup> and 9.1921 mol of OH<sup>-</sup> in steps of 0.091921 mol/step for Simulant #2. The final volume at the end of the modeled reactions of Simulants #1 and #2 were 1519 mL and 1485 mL, respectively.

## 2.9 Quality Assurance

Requirements for performing reviews of technical reports and the extent of review are established in manual E7 2.60. SRNL documents the extent and type of review using the SRNL Technical Report Design Checklist contained in WSRC-IM-2002-00011, Rev. 2.<sup>25</sup> This work was performed following the applicable Task Technical and Quality Assurance Plan (TTQAP).<sup>26</sup> The Technical Task Request (TTR) associated with this work<sup>7</sup> requested a functional classification of Safety Significant (see section 9.5 of the TTQAP entitled “Clarification of Safety Significant Functional Classification”). To match the requested functional classification, this report and calculations within received a technical review by design verification.<sup>27</sup> Data are recorded in the Electronic Laboratory Notebook (ELN) system.<sup>28</sup>

## 3.0 Results and Discussion

### 3.1 Simulant Characterization

As described above, two different starting simulants were prepared for the neutralization studies. The first simulant represents the expected composition of the dissolver solution after dissolution of a HFIR fuel batch and adjustment of the <sup>235</sup>U enrichment level to 3% with Gd added as a neutron poison at a ratio of 0.625:1 Gd:<sup>235</sup>U. The second simulant represents the expected composition of the dissolver solution, again after dissolution of a HFIR batch of fuel and adjustment to 3% enrichment, but also with the addition of Fe as a neutron poison at a ratio of 160:1 Fe:<sup>239</sup>Pu equivalents. After preparation of the simulants, samples were analyzed by ICP-ES and free acid titration. The results are provided in Table 3-1. The metals were within 6% of target as where the HNO<sub>3</sub> was within 19%.

**Table 3-1. Composition of Prepared Simulants**

Component	Simulant #1		Simulant #2	
	Concentration	% of Target	Concentration	% of Target
Al	39.8 g/L	97.5%	14.2 g/L	94.1%
U	76.2 g/L	103%	26.0 g/L	95.3%
Gd	1.41 g/L	102%	0.503 g/L	98.4%
Fe	n/a	n/a	85.0 g/L	99.9%
HNO <sub>3</sub>	1.12 M	85.5%	0.401 M	81.8%
Gd: <sup>235</sup> U ratio	0.617	98.7%	0.645	103%
Fe: <sup>239</sup> Pu <sub>eq</sub>	n/a	n/a	168	105%

### 3.2 Neutralization Reactions

#### 3.2.1 Simulant #1

Neutralization of Simulant #1 was performed as described above, starting with 608 mL of the as-prepared simulant. Sodium hydroxide (50 wt%) was slowly added at a controlled rate using a syringe pump. The starting rate of addition was 2 mL/min, but this was increased to 4 mL/min after the first 70 mL of 50 wt% NaOH had been added. An orange-colored precipitate was formed immediately upon addition of sodium hydroxide. The precipitate appeared to slowly redissolve; however, never fully redissolved given the time frame of observation. It has been previously reported that the presence of a local hydroxide concentration appreciably higher than the overall concentration can lead to the formation of an aluminum precipitate that is difficult to redissolve, even though it is unstable.<sup>29</sup> After 55 mL of 50 wt% NaOH had been added, the NaOH addition and agitation was stopped, and the first sample (2 mL) was collected from the vessel. The pH was measured to be approximately 2 (with pH test strip). The precipitate was observed to settle quickly to the bottom of the vessel during this sampling effort. This sample was filtered to obtain both a liquid and solid phase for analysis. The filtrate was further diluted with DDI water and submitted for ICP-ES analysis.

The solids were easily dissolved in 1 mL of 8 M  $\text{HNO}_3$  and diluted with DDI water prior to submission for ICP-ES analysis. After collection of the sample, the agitator was turned on and the NaOH addition continued. Once 100 mL of 50 wt% NaOH had been added, the addition was again paused to collect a sample (2 mL). At this point in the neutralization process the solids appeared to be more stable and not redissolving, and the measured pH was approximately 2.5. When collecting the 2 mL sample from the vessel it was observed that the precipitate quickly settled in the pipette tip. The sample was filtered, prepared, and submitted for analysis as previously described. A photograph of the solids collected at this second sampling point is shown in Figure 3-1. After collecting the second sample, NaOH addition continued. Upon reaching approximately 190 mL of 50 wt% NaOH added, the mixture became difficult to mix due to the large quantity of solids that had precipitated. The agitator speed was increased from 400 to 1100 rpm in attempts to mix, with no success. A sample of the solid was collected at this point using a spatula. No filtrate/supernate sample could be obtained. The collected solids were dissolved in 8 M  $\text{HNO}_3$ , diluted with DDI water, and submitted for analysis. In this case the solids did not readily dissolve in 1 mL of 8 M  $\text{HNO}_3$  so an additional 0.5 mL was added at which time the solids fully dissolved. A photograph the reaction vessel at this point in the neutralization is shown in Figure 3-2. After collecting the sample, the agitator was raised slightly in the vessel, and the NaOH was continuously added to the shaft location and a cavern was created that slowly increased in size until mixing was observed throughout the surface. Regions at the bottom of the vessel, furthest away from the impeller were still gelled, in this case the vessel was moved to blend in these sections. The NaOH addition continued, and a fluid system was once again obtained as the aluminum began to redissolve. The NaOH addition continued until a total of 291.4 mL of 50 wt% NaOH had been added to achieve a free hydroxide concentration of 0.6 M. At this point, the simulant was roughly equally divided into two polyethylene bottles. The first bottle (0.6 M free hydroxide endpoint) received 450 mL of the neutralized simulant and the second bottle (to become the 1.2 M free hydroxide endpoint) received 456 mL of the neutralized simulant. The 1.2 M free hydroxide endpoint was achieved by adding 15.25 mL of 50 wt% NaOH to the 1.2 M free hydroxide bottle, capping, and then shaking the bottle to mix. Samples were then removed from both bottles, filtered, and samples prepared for analysis. The solids collected in these samples proved more difficult to dissolve than earlier samples and the final acid quantities added to each solids sample to achieve complete dissolution were 3 mL of 8 M  $\text{HNO}_3$  and 1 mL of concentrated (i.e., 15.7 M)  $\text{HNO}_3$ .



**Figure 3-1. Photograph of solids collected on filter from Sample #2 during neutralization of Simulant #1.**



**Figure 3-2. Photograph of the reaction mixture at the point of maximum solids precipitation during neutralization of Simulant #1 (190 mL of 50 wt% NaOH had been added).**

Summaries of the ICP-ES data for the liquid and solid phases of each sample collected are provided in Table 3-2 and Table 3-3, respectively. The row and column of Table 3-2 and 3-3, respectively, shows the Gd:<sup>235</sup>U ratio. The experiments were performed using depleted uranium; and therefore, the theoretical <sup>235</sup>U amount was calculated based upon an enrichment level of 3 wt%. The lowest Gd:<sup>235</sup>U ratio was observed in the solid sample obtained near the equivalence point where maximum solids precipitation was observed. For comparison the Gd:<sup>235</sup>U in the prepared simulant was 0.617 (target of 0.625). The Nuclear Criticality Safety Evaluation (NCSE) calculated the minimum critically safe gadolinium to uranium ratio in an infinite system to be 1:40 weight ratio of Gd to <sup>235</sup>U with all credible hydrogen to fissile atom ratios.<sup>30</sup> This is a 0.025 Gd:<sup>235</sup>U ratio. Therefore, all sampling points taken throughout the neutralization are well within the safety limits based on the NCSE.

**Table 3-2. Supernate Component Concentrations During Neutralization of Simulant #1**

Sample		1	2	3	4 (0.6 M OH <sup>-</sup> )	5 (1.2 M OH <sup>-</sup> )
mL 50 wt% NaOH added		55	100	190	291.4	321.4 <sup>a</sup>
moles NaOH Added		1.04	1.89	3.60	5.52	6.09 <sup>a</sup>
Measured (Calculated <sup>b</sup> ) pH		~2 (2.8)	~2.5 (2.9)	NM (3.2)	NM (13.8)	NM (14.1)
Al	g/L <sup>c</sup>	34.6	32.3	— <sup>d</sup>	11.9	18.7
	% Original	95%	94%	— <sup>d</sup>	44%	72%
Gd	g/L <sup>c</sup>	1.18	1.09	— <sup>d</sup>	< 9.0E-04	< 9.0E-04
	% Original	91%	90%	— <sup>d</sup>	< 0.09%	< 0.10%
U	g/L <sup>c</sup>	67.0	61.5	— <sup>d</sup>	< 0.014	< 0.014
	% Original	96%	94%	— <sup>d</sup>	< 0.03%	< 0.03%
Gd: <sup>235</sup> U <sup>e</sup>		0.585	0.591	— <sup>d</sup>	n/a	n/a

NM = not measured. <sup>a</sup> This is the equivalent amount that would have been added had the slurry not been split once reaching the 0.6 M free hydroxide endpoint. The actual amount was less due the smaller actual volume adjusted to 1.2 M free hydroxide. <sup>b</sup> OLI Studio 9.6 was used to calculate the pH at sampling points 1-3. The calculated pH of points 4 and 5 is the calculated pH of 0.6 and 1.2 M hydroxide, respectively. <sup>c</sup> The analytical uncertainty for the ICP-ES results is 10% at 2 sigma. <sup>d</sup> No supernate sample obtained at this point. <sup>e</sup> Testing was performed with depleted U; however, this is the calculated Gd:<sup>235</sup>U ratio assuming an enrichment of 3%.

**Table 3-3. Solid Component Concentrations During Neutralization of Simulant #1**

Sample	1	2	3	4 (0.6 M OH <sup>-</sup> )	5 (1.2 M OH <sup>-</sup> )
mL 50 wt% NaOH added	55	100	190	291.4	321.4 <sup>a</sup>
moles NaOH Added	1.04	1.89	3.60	5.52	6.09 <sup>a</sup>
Al (g/L) <sup>b</sup>	9.55	8.49	7.25	9.75	6.55
Gd (g/L) <sup>b</sup>	0.330	0.255	0.233	0.372	0.318
U (g/L) <sup>b</sup>	18.7	15.1	14.2	20.6	17.2
Gd: <sup>235</sup> U <sup>c</sup>	0.589	0.563	0.549	0.602	0.617

<sup>a</sup> This is the equivalent amount that would have been added had the slurry not been split once reaching the 0.6 M free hydroxide endpoint. The actual amount was less due the smaller actual volume adjusted to 1.2 M free hydroxide. <sup>b</sup> Comparison of absolute concentrations between samples is not relevant due to different amounts of solids collected and different amounts of acid used to dissolve solids. The analytical uncertainty for the ICP-ES results is 10% at 2 sigma. <sup>c</sup> Testing was performed with depleted U; however, this is the calculated Gd:<sup>235</sup>U ratio assuming an enrichment of 3%.

### 3.2.2 Simulant #2

Neutralization of Simulant #2 was performed as described above, starting with 610 mL of the as-prepared simulant. Sodium hydroxide (50 wt%) was slowly added at a controlled rate with the use of a syringe pump at a rate of 4 mL/min. A precipitate was observed immediately upon addition of sodium hydroxide. Sodium hydroxide addition continued, and the solution was observed to become darker in color as the addition continued with the precipitation of dark brown solids. Sodium hydroxide addition was paused when 50 mL of 50 wt% NaOH had been added, at which point the first sample (2 mL) was collected from the vessel and the pH was measured to be < 1 (with pH test strip). This sample was filtered to obtain a liquid and solid phase for analysis. The filtrate was further diluted in water and submitted for ICP-ES analysis, and the solid was easily dissolved in 0.5 mL of 8 M HNO<sub>3</sub>. The dissolved solids solution was also diluted in water prior to submission for ICP-ES analysis. After collection of the sample, the NaOH addition continued. At the point where approximately 100 mL of 50 wt% NaOH had been added, the rotor speed was increased from 300 rpm to 350 rpm to maintain a slight vortex. Once 150 mL of 50 wt% NaOH had been added, the addition was again paused to collect a sample (2 mL). It was found that the pH was difficult to read due to the dark color of the solution staining the pH test strips; however, the pH appeared to still be < 2 at the second sampling point. Again, the sample was filtered, and the solids collected were easily dissolved in 1 mL of 8 M HNO<sub>3</sub>. Diluted samples of the filtrate and dissolved solids were again submitted for analysis. After collecting the second sample, NaOH addition continued. As the mixture became more viscous due to the precipitation of a large quantity of solids, the rotor speed was increased 50 rpm at a time from 350 rpm to 550 rpm by the time 210 mL of 50 wt% NaOH had been added. Upon reaching 225 mL of 50 wt% NaOH added, the mixture became difficult to mix and the rotor speed had been increased to 800 rpm. The third sample was collected at this point. A 2 mL sample was removed from near the surface to obtain a liquid fraction. The sample was filtered, and a small amount of filtrate was obtained for analysis, although the sample was difficult to filter and could not all be filtered. A small sample of the solids was collected directly on the tip of a spatula and this sample was easily dissolved in 1 mL of 8 M HNO<sub>3</sub>. After collecting the samples, the NaOH addition was resumed. The mixture remained viscous and difficult to mix, and the agitator speed was increased to 900 rpm. As additional NaOH was added, and the mixture became more fluid the agitator speed was reduced to 800 rpm and then to 700 rpm. The NaOH addition continued until a total of 270 mL of 50 wt% NaOH had been added to achieve a free hydroxide concentration of 0.6 M. Once reaching the 0.6 M free hydroxide end point, the reaction mixture was roughly equally divided into two polyethylene bottles. The first bottle (0.6 M free hydroxide endpoint) received 440 mL of the slurry and the second bottle (to become the 1.2 M free hydroxide endpoint) received 438 mL of the slurry. It was also observed that the Simulant #2 solids are more cohesive than Simulant #1 and more of the solids remained in the mixing vessel. An additional 12.9 mL of 50 wt% NaOH was then added to the 1.2 M free hydroxide bottle and the contents were mixed by capping and shaking the bottle. Samples were then removed from both bottles to prepare for analysis. Filtration of samples from either endpoint was

unsuccessful, and therefore samples from each endpoint were centrifuged in a minicentrifuge to separate the solid and liquid fractions. The supernate was decanted and diluted for analysis, and a portion of the solids from each endpoint were dissolved in 0.5 mL of 8 M HNO<sub>3</sub> and 0.5 mL of concentrated HNO<sub>3</sub>.

Summaries of the ICP-ES data for the liquid and solid phases of each sample collected are provided in Table 3-4 and Table 3-5, respectively, including the calculated Gd:<sup>235</sup>U and Fe:<sup>239</sup>Pu<sub>eq</sub> ratios. The experiments were performed using depleted uranium; and therefore, the theoretical <sup>235</sup>U amount was calculated based upon the assumed enrichment level of 3 wt%. For this simulant, the lowest Gd:<sup>235</sup>U ratio was observed in the solid sample obtained when 150 mL of 50 wt% NaOH had been added. In agreement with that, the highest Gd:<sup>235</sup>U ratio was observed in the filtrate from that same sampling point, indicating that a larger percentage of U than of the Gd had precipitated at that point during the neutralization. The Gd:<sup>235</sup>U in the prepared simulant was 0.645 (target of 0.625). Similar to the discussion of the neutralization of Simulant #1, all sampling points taken throughout the neutralization are well within the safety limits based on the NCSE.<sup>30</sup> The Fe:<sup>239</sup>Pu<sub>eq</sub> ratio was slightly below the target of 160 in the liquid phase at the first two sampling points. For sampling points 3 – 5 the U concentration in the supernate was below the method detection limit. As seen in Table 3-5, the Fe:<sup>239</sup>Pu<sub>eq</sub> ratio remained above 160 in the solids obtained at each sampling point. The highest Fe:<sup>239</sup>Pu<sub>eq</sub> ratio was seen in the solids of sample 2, and correspondingly the lowest ratio was observed in the supernate from sample 2.

**Table 3-4. Supernate Component Concentrations During Neutralization of Simulant #2**

Sample		1	2	3	4 (0.6 M OH <sup>-</sup> )	5 (1.2 M OH <sup>-</sup> )
mL 50 wt% NaOH added		50	150	225	270	295.8 <sup>a</sup>
moles NaOH Added		0.947	2.84	4.26	5.11	5.60 <sup>a</sup>
Measured (Calculated <sup>b</sup> ) pH		<1 (1.2)	<2 (1.5)	NM (12.8)	NM (13.8)	NM (14.1)
Al	g/L <sup>c</sup>	13.9	10.6	4.88	6.96	7.98
	% Original	106%	93%	47%	71%	83%
Fe	g/L <sup>c</sup>	72.5	47.8	0.147	0.0239	0.0196
	% Original	92%	70%	0.24%	0.041%	0.0343%
Gd	g/L <sup>c</sup>	0.464	0.355	< 0.00304	< 0.00107	< 0.00107
	% Original	100%	88%	< 0.83%	< 0.31%	< 0.32%
U	g/L <sup>c</sup>	23.6	16.9	<0.106	< 0.0376	< 0.0376
	% Original	98%	81%	< 0.56%	< 0.21%	< 0.21%
Gd: <sup>235</sup> U <sup>d</sup>		0.657	0.700	n/a	n/a	n/a
Fe: <sup>239</sup> Pu <sub>eq</sub> <sup>e</sup>		158	145	> 70.8	> 32.6	> 26.8

<sup>a</sup> This is the equivalent amount that would have been added had the slurry not been split once reaching the 0.6 M free hydroxide endpoint. The actual amount was less due the smaller actual volume adjusted to 1.2 M free hydroxide. <sup>b</sup> OLI Studio 9.6 was used to calculate the pH at sampling points 1-3. The calculated pH of points 4 and 5 is the calculated pH of 0.6 and 1.2 M hydroxide, respectively. <sup>c</sup> The analytical uncertainty for the ICP-ES results is 10% at 2 sigma. <sup>d</sup> Testing was performed with depleted U; however, this is the calculated Gd:<sup>235</sup>U ratio assuming an enrichment of 3%. <sup>e</sup> Testing was performed with depleted U; however, this is the calculated Fe:<sup>239</sup>Pu<sub>eq</sub> ratio assuming a U enrichment of 3% and using equation (1) to calculate the <sup>239</sup>Pu<sub>eq</sub>. NM = not measured.

**Table 3-5. Solid Component Concentrations During Neutralization of Simulant #2**

Sample	1	2	3	4 (0.6 M OH <sup>-</sup> )	5 (1.2 M OH <sup>-</sup> )
mL 50 wt% NaOH added	50	150	225	270	295.8 <sup>a</sup>
moles NaOH Added	0.947	2.84	4.26	5.11	5.60 <sup>a</sup>
Al (g/L) <sup>b</sup>	4.52	3.53	1.43	1.69	1.58
Fe (g/L) <sup>b</sup>	25.7	22.7	7.50	10.6	11.2
Gd (g/L) <sup>b</sup>	0.145	0.0942	0.0447	0.0509	0.0557
U (g/L) <sup>b</sup>	7.86	5.69	2.38	2.90	3.30
Gd: <sup>235</sup> U <sup>c</sup>	0.614	0.552	0.625	0.586	0.562
Fe: <sup>239</sup> Pu <sub>eq</sub> <sup>d</sup>	168	205	162	187	173

<sup>a</sup> This is the equivalent amount that would have been added had the slurry not been split once reaching the 0.6 M free hydroxide endpoint. The actual amount was less due the smaller actual volume adjusted to 1.2 M free hydroxide. <sup>b</sup> Comparison of absolute concentrations between samples is not relevant due to different amounts of solids collected and different amounts of acid used to dissolve solids. The analytical uncertainty for the ICP-ES results is 10% at 2 sigma. <sup>c</sup> Testing was performed with depleted U; however, this is the calculated Gd:<sup>235</sup>U ratio assuming an enrichment of 3%. <sup>d</sup> Testing was performed with depleted U; however, this is the calculated Fe:<sup>239</sup>Pu<sub>eq</sub> ratio assuming a U enrichment of 3% and using equation (1) to calculate the <sup>239</sup>Pu<sub>eq</sub>.

### 3.3 Physical Property Measurements

#### 3.3.1 As-Batched

Triplicate samples of the slurry from each neutralization endpoint (0.6 M and 1.2 M free hydroxide) were collected for solids analysis after mixing well. The total solids in the sample and soluble solids in the supernate were measured and used to calculate the insoluble solids present in the sample, using equation (3). Triplicate density measurements of each slurry were made. The %RSD is determined by calculating the standard deviation and dividing this value by the average. A summary of the results is provided in Table 3-6. Simulant #1 at the 0.6 M free OH<sup>-</sup> endpoint contained the largest fraction of insoluble solids. For each simulant, the wt%<sub>IS</sub> decreased with increasing hydroxide concentration, consistent with increased solubility of the aluminum at higher hydroxide concentration. The densities of all the “as-batched” simulants exceeded the 1.35 g/mL limit.

**Table 3-6. Weight Percent Solids Concentrations and Densities of Endpoint Simulants**

	wt% Total Solids		wt % Soluble Solids		wt% Insoluble Solids		Density (g/mL)	
	Average	%RSD <sup>a</sup>	Average	%RSD <sup>a</sup>	Average	%RSD <sup>a</sup>	Average	%RSD <sup>a</sup>
<b>Simulant #1 0.6 M OH<sup>-</sup></b>	41.6	0.44	35.0	0.40	10.2	0.90	1.377	0.12
<b>Simulant #1 1.2 M OH<sup>-</sup></b>	43.1	0.91	37.1	0.24	9.64	5.65	1.385	0.05
<b>Simulant #2 0.6 M OH<sup>-</sup></b>	41.6	0.30	34.8	3.74	9.02	7.52	1.368	0.21
<b>Simulant #2 1.2 M OH<sup>-</sup></b>	41.3	1.03	36.6	0.65	7.45	12.6	1.373	0.40

<sup>a</sup> Percent relative standard deviation from triplicate measurements.

Particle size analysis was performed on a sample from each of the four endpoints. The volumetric particle size distributions are shown in Figure 3-3 and Figure 3-4 and percentiles are summarized in Table 3-7. The particle size distributions for Simulant #2 samples are narrower, containing no submicron size particles. Simulant #1 samples have a bimodal distribution. The minimum particle size observed for the Simulant #2 samples was 2.3 μm versus 0.49 μm for the Simulant #1 samples. The maximum particle sizes observed for the Simulant #2 samples were 22.0 μm and 37 μm compared to 31.1 μm and 44.0 μm for the Simulant #1 0.6 M and 1.2 M free OH<sup>-</sup> endpoints, respectively. These particle sizes are small enough that the Gd self-shielding should be minimized (general guideline is less than 100 μm to minimize self-shielding).<sup>31</sup> The Simulant #1 samples were observed to settle to a much more compact volume in comparison to the

Simulant #2 samples. A photograph taken after several days of settling is shown in Figure 3-5. The difference observed in the levels of settling could be due to the electrical double shell around the solids from the ionic fluid and/or the particle size distribution. Settling rates were not measured; however, during the 1<sup>st</sup> rheological measurements (approximately 12 minutes), the 2<sup>nd</sup> aliquot of sample (awaiting measurement) was observed visually, and no clear liquid interface developed in these samples.

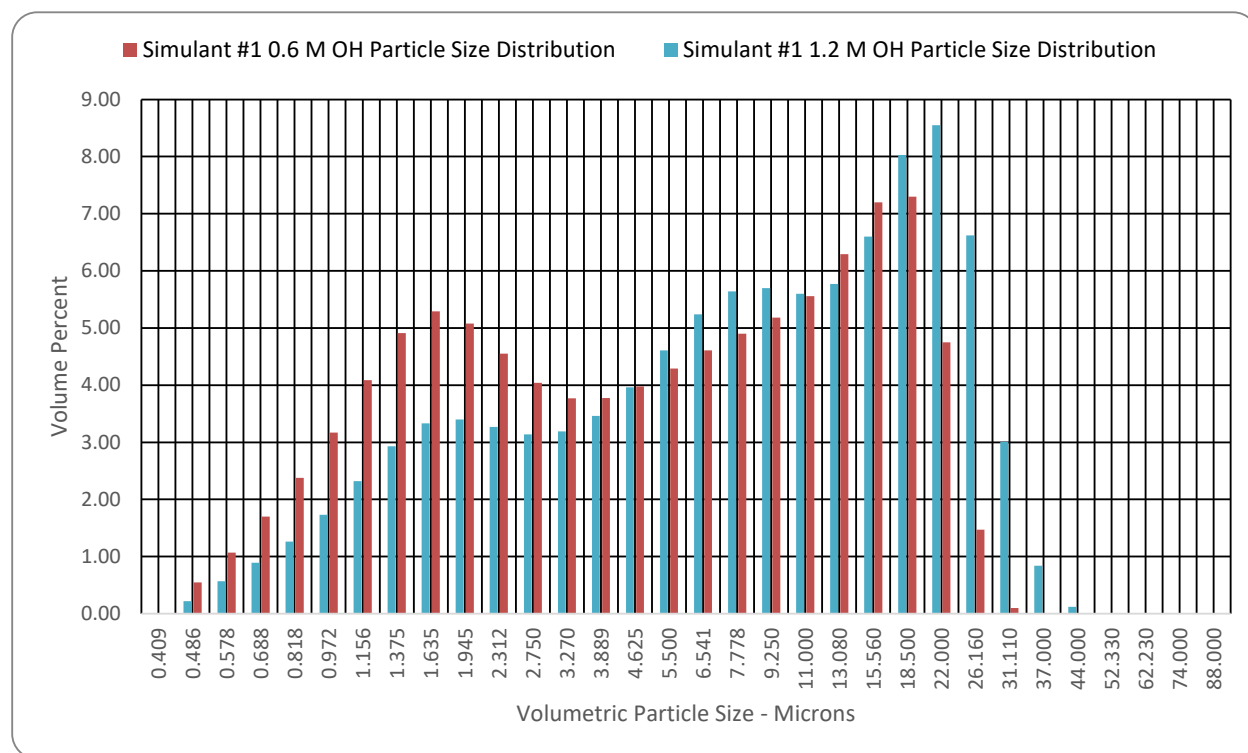


**Figure 3-3. Volumetric Particle Size Distribution for Simulant #1 Endpoints.**

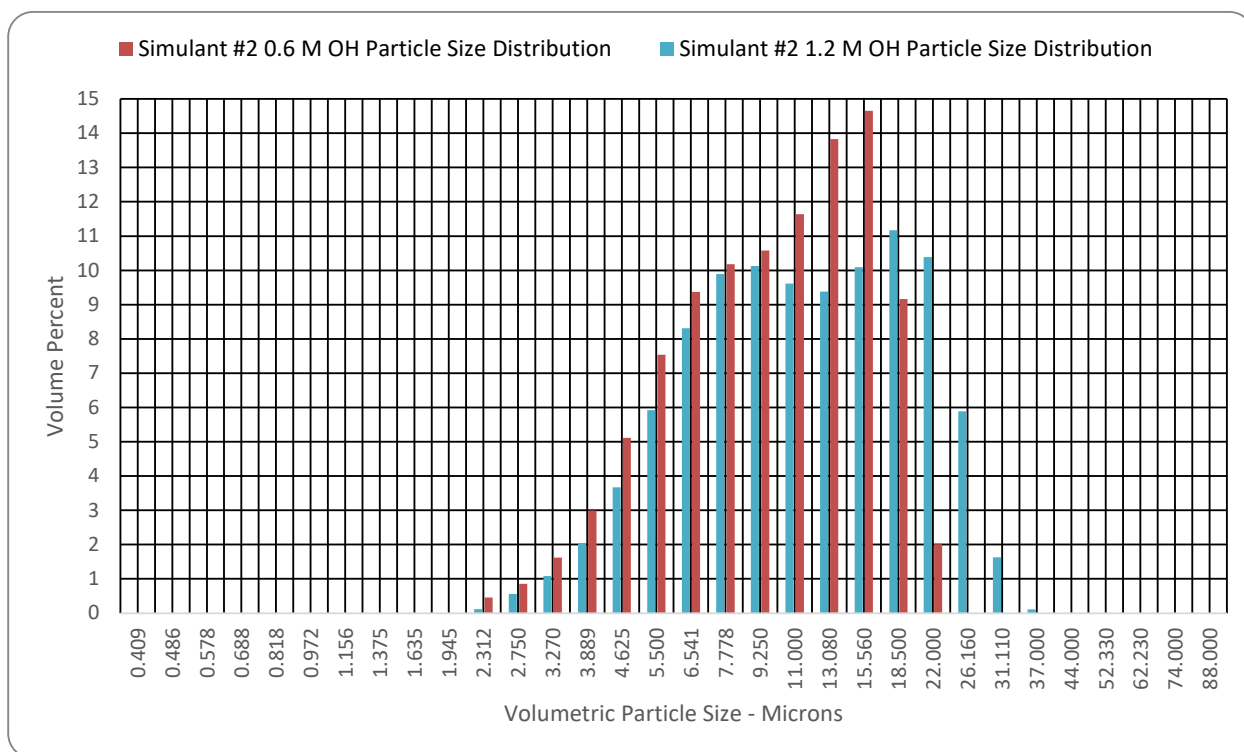


**Figure 3-4. Volumetric Particle Size Distribution for Simulant #2 Endpoints.**

**Table 3-7. Particle Size Distribution Data for Simulants #1 and #2 Endpoints**

Volume Percentile	Simulant #1 0.6 M OH (μm)	Simulant #1 1.2 M OH (μm)	Simulant #2 0.6 M OH (μm)	Simulant #2 1.2 M OH (μm)
10	1.024	1.381	4.49	5.02
20	1.475	2.322	5.65	6.33
30	2.075	3.94	6.78	7.57
40	3.18	5.83	8.03	8.98
50	4.95	7.98	9.44	10.73
60	7.22	10.85	10.95	12.91
70	10.08	14.50	12.45	15.36
80	13.36	18.18	13.98	17.95
90	16.89	22.30	15.83	21.04
95	19.23	25.31	17.21	23.41
Mean <sup>a</sup>	7.15	10.23	9.84	12.07

<sup>a</sup> Mean diameter of the volume distribution =  $D_{3/2} = \frac{\sum vol\%_i \cdot D_i^3}{\sum vol\%_i \cdot D_i^2}$



**Figure 3-5. Photograph of bottles containing product from each neutralization. From left to right: Simulant #1, 0.6 M OH<sup>-</sup>; Simulant #1, 1.2 M OH<sup>-</sup>; Simulant #2, 0.6 M OH<sup>-</sup>; Simulant #2, 1.2 M OH<sup>-</sup>.**

### 3.3.2 Targeted Densities Results

The target density simulants for rheology were batched based on the volumes stated in Table 2-8. These target density simulants were prepared, characterized for rheology using the VT550, and finally the density was measured. To determine the wt%<sub>TS</sub> and wt%<sub>IS</sub> (total, Na<sub>2</sub>U<sub>2</sub>O<sub>7</sub>, and Gd(OH)<sub>3</sub>) in the target density simulants, the densities of the 0.6 M and 1.2 M NaOH solutions and their corresponding wt%<sub>TS</sub> were used (Table 3-8) with the measured target density of each simulant, the volumes stated in Table 2-8, and the use of equations (6) and (7). Each flow curve was fitted with the Bingham Plastic model between a shear rate of 100 to 600 sec<sup>-1</sup> for both the up and down curves. Additionally, the viscosity at 600 sec<sup>-1</sup> was averaged. The data for Simulant #1 is provided in Table 3-9. For Simulant #2, Table 3-10 and Table 3-11 are provided for the 0.6 M and 1.2 M target density samples, respectively. The flow curve shows that the up curves have a slightly larger yield stress and slightly lower plastic viscosity as compared to the down curve. This is due to inertia effects of accelerating (up curve) and decelerating (down curve) of the MV1 rotor. For Simulant #1, the viscosity at 600 sec<sup>-1</sup> is within 21% of the corresponding plastic viscosity, indicating the yield stress is not a large contributor. This is not the case for Simulant #2, where the viscosity is 20 to 60% greater than the plastic viscosity and increases as the sample density increases, in this case the yield stress is a factor.

**Table 3-8. Density and Weight Percent Total Solids of Diluents**

Molarity	Density (g/mL)	wt% <sub>TS</sub>
0.6	1.025	3.10
1.2	1.050	5.37

**Table 3-9. Density, Wt%<sub>TS</sub>, Wt%<sub>IS</sub>, and Rheology Results for Simulant #1 Target Density Samples**

Properties		0.6 M OH				1.2 M OH			
Density (g/mL)	Target	1.35	1.33	1.31	1.27	1.35	1.33	1.31	1.27
	Measured	1.355	1.336	1.317	1.279	1.354	1.331	1.317	1.278
	% RSD	0.09	0.09	0.09	0.05	0.12	0.08	0.01	0.02
Solids	wt% <sub>TS</sub>	39.2	37.5	35.7	31.9	40.0	38.2	36.2	32.3
	wt% <sub>IS</sub>	9.53	9.07	8.61	7.61	8.85	8.37	7.88	6.87
	wt% <sub>Na<sub>2</sub>U<sub>2</sub>O<sub>7</sub></sub>	4.72	4.49	4.26	3.77	4.08	3.86	3.63	3.16
	wt% <sub>Gd(OH)<sub>3</sub></sub>	0.09	0.08	0.08	0.07	0.08	0.07	0.07	0.06
Bingham Plastic	Up curve	$\tau_o$ (Pa)	0.41	0.38	0.34	0.29	0.36	0.31	0.25
		%RSD	0.70	14	1.4	3.0	19	12	18
		$\mu_{\infty}$ (cP)	4.3	3.8	3.5	3.0	4.5	3.9	3.1
		% RSD	4.1	3.9	0.61	0.71	0.71	2.0	3.6
	Down curve	$\tau_o$ (Pa)	0.22	0.23	0.18	0.14	0.25	0.12	0.085
		%RSD	3.2	5.5	14	18	28	40	63
		$\mu_{\infty}$ (cP)	4.5	3.8	3.6	3.1	4.5	4.1	3.7
		% RSD	3.6	1.2	1.4	1.6	0.44	2.1	1.7
Newtonian at 600s <sup>-1</sup>	Visc (cP)	4.9	4.3	3.9	3.6	5.0	4.4	3.9	3.6
	% RSD	2.9	2.9	0.49	1.3	2.7	0.89	4.0	3.1

**Table 3-10. Density, Wt%<sub>TS</sub>, Wt%<sub>IS</sub>, and Rheology Results for Simulant #2, 0.6 M Target Density Samples**

Properties		0.6 M OH					
Density (g/mL)	Target	1.35	1.33	1.31	1.29	1.25	1.21
	Measured	1.353	1.328	1.309	1.289	1.258	1.220
	% RSD	0.29	0.38	0.34	0.10	0.28	0.22
Solids	wt% <sub>TS</sub>	40.0	38.4	36.6	34.7	30.6	27.7
	wt% <sub>IS</sub>	8.65	8.27	7.83	7.39	6.44	5.46
	wt% Na <sub>2</sub> U <sub>2</sub> O <sub>7</sub>	1.75	1.67	1.58	1.50	1.30	1.10
	wt% Gd(OH) <sub>3</sub>	0.05	0.05	0.05	0.05	0.04	0.03
Bingham Plastic	Up curve	$\tau_o$ (Pa)	3.6	3.0	2.2	1.8	0.90
		%RSD	2.5	7.1	3.3	4.7	25
		$\mu_{\infty}$ (cP)	9.8	8.3	6.4	5.4	4.1
		% RSD	3.6	2.5	0.0	1.4	1.9
	Down curve	$\tau_o$ (Pa)	3.0	2.4	1.6	1.5	0.73
		%RSD	6.6	4.1	3.8	4.5	1.8
		$\mu_{\infty}$ (cP)	10	8.9	7.0	5.8	4.4
		% RSD	2.1	0.40	0.30	1.8	1.4
Newtonian at 600s <sup>-1</sup>	Visc (cP)	16	13	9.9	8.3	5.7	3.9
	% RSD	0.30	1.7	0.67	2.2	0.58	0.30

**Table 3-11. Density, Wt%<sub>TS</sub>, Wt%<sub>IS</sub>, and Rheology Results for Simulant #2, 1.2 M Target Density Samples**

Properties		1.2 M OH						
Density (g/mL)	Target	1.35	1.33	1.31	1.29	1.25	1.21	
	Measured	1.354	1.333	1.310	1.289	1.257	1.223	
	% RSD	0.31	0.29	0.38	0.39	0.20	0.10	
Solids	wt% <sub>TS</sub>	39.2	37.4	35.6	33.8	29.6	26.9	
	wt% <sub>IS</sub>	7.02	6.65	6.28	5.90	5.04	4.15	
	wt% <sub>Na<sub>2</sub>U<sub>2</sub>O<sub>7</sub></sub>	1.52	1.44	1.36	1.28	1.09	0.90	
	wt% <sub>Gd(OH)<sub>3</sub></sub>	0.05	0.04	0.04	0.04	0.03	0.03	
Bingham Plastic	Up curve	$\tau_o$ (Pa)	2.1	1.8	1.5	1.2	0.75	0.44
		%RSD	2.7	5.9	8.1	- <sup>a</sup>	2.5	3.9
		$\mu_{\infty}$ (cP)	9.4	7.8	6.2	5.2	4.0	3.2
		% RSD	2.0	0.91	4.4	- <sup>a</sup>	0.88	1.1
	Down curve	$\tau_o$ (Pa)	1.6	1.4	1.1	0.90	0.45	0.22
		%RSD	1.9	9.4	4.0	- <sup>a</sup>	4.7	9.0
		$\mu_{\infty}$ (cP)	9.9	8.2	6.7	5.6	4.3	3.3
		% RSD	3.2	2.1	1.2	- <sup>a</sup>	1.8	1.5
Newtonian at 600s <sup>-1</sup>	Visc (cP)	13	11	8.6	7.1	5.2	3.8	
	% RSD	1.4	1.2	0.51	- <sup>a</sup>	1.3	0.0	

<sup>a</sup> 2<sup>nd</sup> flow curve was not zeroed, one data set reported

### 3.4 Flow Calculations

Flow calculations were performed for lines 1100 and 1102, though the discussions are focused on 1100. Pipe roughness of 0.00015 ft (clean), 0.00125 ft (light rust), and 0.00667 ft (general rust) were analyzed for a majority when assessed as a Newtonian fluid. The expected flow of the steam jets to the 10-inch header is 75 gpm.<sup>32</sup>

The flowrate results for Simulant #1 are provided in Table 3-12. Below is a summary of the results for line 1100.

- For the range of target densities 1.27 to 1.35 g/mL,
  - Non-Newtonian flowrate ranged between 98 to 102 gpm.
  - Pipe roughness 0.00015 ft, flowrate ranged between 87 to 89 gpm
  - Pipe roughness 0.00125 ft, flowrate ranged between 76 to 77 gpm
  - Pipe roughness 0.00667 ft, flowrate was approximately 59 gpm
- Flow is turbulent for all cases.
- In many cases the pipe will be partially full given the capacity is greater than the feed rate.
- Header will start backing up when pipe roughness is greater than 0.00125 ft.
- The facility can process Simulant #1 to the 10" header for any density below 1.35 g/mL.
- To minimize unnecessary fluid addition, target 1.35 g/mL.

For Simulant #2, the flowrates for the 0.6 M are provided in Table 3-13 and the 1.2 M in Table 3-14. Below is a summary of the results for line 1100.

- 0.6 M (Table 3-13)
  - For the range of target densities 1.21 to 1.35 g/mL

- Non-Newtonian flowrate ranged between 80 to 101 gpm
  - Pipe roughness 0.00015 ft, flowrate ranged between 75 to 88 gpm
  - Pipe roughness 0.00125 ft, flowrate ranged between 69 to 76 gpm
  - Pipe roughness 0.00667 ft, flowrate was approximately 57 to 60 gpm
- Densities 1.25 and 1.21 g/mL similar flowrate to Simulant #1
  - Non-Newtonian; 99 to 101 gpm.
  - 0.00015 ft roughness; 85 to 88 gpm
  - 0.00125 ft roughness; 74 to 76 gpm
- Non-Newtonian case for 1.35 and 1.33 g/mL indicate condition of flow to be slightly greater than laminar. For lower densities, the impact of roughness and turbulence is unknown to properly assess pressure drop.
- When analyzed as a Newtonian fluid, for clean pipe, all conditions are acceptable for processing. When the pipe roughness is 0.00125 ft, densities greater than 1.21 g/mL indicate the fluid will start backing into the header. For pipe roughness of 0.00667 inches, the header will backup for all cases.
- 1.2 M (Table 3-14)
  - For the range of target densities 1.21 to 1.35 g/mL
    - Non-Newtonian flowrate ranged between 92 to 101 gpm
    - Pipe roughness 0.00015 ft, flowrate ranged between 77 to 88 gpm
    - Pipe roughness 0.00125 ft, flowrate ranged between 70 to 76 gpm
    - Pipe roughness 0.00667 ft, flowrate was approximately 58 to 60 gpm
  - Densities 1.25 and 1.21 g/mL similar flowrate to Simulant #1
    - Non-Newtonian; 98 to 101 gpm.
    - 0.00015 ft roughness; 86 to 88 gpm
    - 0.00125 ft roughness; 75 to 76 gpm
  - Non-Newtonian case for 1.35 g/mL indicate condition of flow to be slightly greater than laminar. For lower densities, the impact of roughness and turbulence is unknown to properly assess pressure drop.
  - When analyzed as a Newtonian fluid, for clean pipe, all conditions are acceptable for processing. When the pipe roughness is 0.00125 ft, densities greater than 1.25 g/mL indicate the fluid will start backing into the header. For pipe roughness of 0.00667 inches, the header will backup for all cases.
- For the Newtonian analysis, all measured densities can be processed for clean pipe. As the pipe roughness increased to 0.00125 feet, only the 1.21 g/mL for the 0.6 M and 1.25 g/mL or less for 1.2 M slurries can be process without having the header back up. For larger pipe roughness, expect the header to back up. Reference 15 provides a method to estimate how much volume could backup during a transfer. The bubbler system in the 10" header can be assessed for this problem.
- If treated as non-Newtonian fluids, recommend processing fluids 0.6 M at 1.33 g/mL or greater and 1.2 M at 1.35 g/mL, given these conditions are near laminar flow conditions. At lower densities, the flow may be turbulent where the pressure losses would be greater and the impact of roughness must be considered, such is not captured in the non-Newtonian analysis.

Flushing using water (or slightly acidic solution) at a flowrate of 75 gpm or greater after the slurry transfer is completed is recommended.

**Table 3-12. Flowrates for Simulant #1**

Properties		0.6 M OH <sup>-</sup>				1.2 M OH <sup>-</sup>			
Density (g/mL)	Target	1.35	1.33	1.31	1.27	1.35	1.33	1.31	1.27
	Measured	1.355	1.336	1.317	1.279	1.354	1.331	1.317	1.278
Bingham Plastic Up Curve	$\tau_o$ (Pa)		0.41	0.38	0.34	0.29	0.36	0.31	0.28
	$\mu_{\infty}$ (cP)		4.3	3.8	3.5	3.0	4.5	3.9	3.7
	$N_{ReB,C}$		8304	8909	9062	9391	7738	8097	8053
	Line 1100	Q (gpm)	99.4	100.3	100.7	101.5	99.4	100.1	100.5
		$N_{ReB}$	31727	36449	39054	44205	30468	34841	36506
	Line 1102	Q (gpm)	89.0	89.7	90.2	90.9	88.9	89.6	90.0
		$N_{ReB}$	28399	32632	34970	39592	27272	31193	32688
Newtonian	$\mu_{600\frac{1}{s}}$ (cP)		4.9	4.3	3.9	3.6	5.0	4.4	3.9
	Roughness (ft)	Line	Q (gpm)						
	0.00015	1100	86.8	88.0	88.6	89.0	86.6	87.7	88.6
		1102	77.4	78.5	79.0	79.5	77.2	78.3	79.1
	0.00125	1100	75.9	76.4	76.6	76.8	75.9	76.3	76.7
		1102	68.1	68.6	68.8	69.0	68.1	68.5	68.8
	0.00667	1100	59.4	59.6	59.6	59.6	59.4	59.5	59.6

**Table 3-13. Flowrates for Simulant #2, 0.6 M OH<sup>-</sup>**

Properties		0.6 M OH <sup>-</sup>					
Density (g/mL)	Target	1.35	1.33	1.31	1.29	1.25	1.21
	Measured	1.353	1.328	1.309	1.289	1.258	1.220
Bingham Plastic Up Curve	$\tau_o$ (Pa)		3.61	2.97	2.16	1.83	0.90
	$\mu_{\infty}$ (cP)		9.8	8.3	6.4	5.4	4.1
	$N_{ReB,C}$		10073	10532	11211	11875	11332
	Line 1100	Q (gpm)	79.5	88.0	93.4	95.3	99.0
		$N_{ReB}$	11039	14347	19411	23198	32471
	Line 1102	Q (gpm)	36.3	70.5	81.8	84.2	88.5
		$N_{ReB}$	4719	11344	16979	20484	29014
Newtonian	$\mu_{600\frac{1}{s}}$ (cP)		15.6	13.0	9.9	8.3	5.7
	Roughness (ft)	Line	Q (gpm)				
	0.00015	1100	74.7	76.5	79.3	80.9	84.6
		1102	65.8	67.5	70.0	71.5	74.8
	0.00125	1100	69.0	70.2	71.8	72.7	74.5
		1102	62.0	63.1	64.7	65.5	67.2
	0.00667	1100	57.4	57.9	58.4	58.7	59.2

**Table 3-14. Flowrates for Simulant #2, 1.2 M OH**

Properties		1.2 M OH <sup>-</sup>					
Density (g/mL)	Target	1.35	1.33	1.31	1.29	1.25	1.21
	Measured	1.354	1.333	1.310	1.289	1.257	1.223
Bingham Plastic Up Curve	$\tau_o$ (Pa)	2.07	1.80	1.46	1.24	0.75	0.44
	$\mu_{\infty}$ (cP)	9.4	7.8	6.2	5.2	4.0	3.2
	$N_{ReB,C}$	8550	9274	9988	10616	10643	10325
	Line 1100	Q (gpm)	91.7	92.7	94.7	96.1	98.3
		$N_{ReB}$	13464	16436	20525	24394	31797
	Line 1102	Q (gpm)	80.6	82.7	84.8	86.2	88.5
		$N_{ReB}$	11824	14547	18258	21742	28430
Newtonian	$\mu_{600\frac{1}{s}}$ (cP)	12.7	10.7	8.6	7.1	5.2	3.8
	Roughness (ft)	Line	Q (gpm)				
	0.00015	1100	76.9	78.7	80.8	82.6	85.5
		1102	67.9	69.5	71.4	73.0	75.7
	0.00125	1100	70.4	71.5	72.6	73.6	74.9
		1102	63.4	64.3	65.5	66.4	67.6
	0.00667	1100	57.9	58.3	58.7	58.9	59.3

### 3.5 Critical Velocity

Critical velocities were calculated for all Simulant #1 densities and for Simulant #2, the 1.25 and 1.21 g/mL densities given these conditions can be treated as Newtonian fluids. Table 3-15 contains the wt. % and vol. %  $\text{Na}_2\text{U}_2\text{O}_7$  and the critical velocities for full pipe conditions. The Poloski correlation provides the lowest critical velocity for all conditions. The 30% margin applied to the Wilson and Judge prediction for Simulant #1 shows that for the average pipe velocity (3.25 ft/s), it is sufficient to maintain the solids suspended for all conditions. This is not the case for Simulant #2, for the 1.21 g/mL 0.6 M condition, the 30% margin exceeded the average velocity. For Simulant #2, 1.2 M, the 30% margin was exceeded.

For the partial flow calculations, only the extreme density conditions were analyzed for both Simulant #1 and #2, given they bound the results as was shown in Table 3-15. The slope required to maintain 75 gpm is also provided in Table 3-16, which is greater than most of the piping as discussed in section 2.7, indicating most of the piping is under full flow conditions. In section 3.4, the calculations showed there is excess capacity in line 1100, such that the available hydraulic head can easily handle 75 gpm and is supported by the required slope for 75 gpm in Table 3-16, which are all smaller than the average slope. For the average slope condition, the pipe is not full, resulting in an average velocity in excess of 4 ft/sec with a slight increase in the critical velocity due to the hydraulic radius being slightly larger. For such conditions, the average velocity is greater than the critical velocity for all conditions, unlike the full pipe condition. Sloped lines would further mitigate solids settle to the bottom of the pipe.

**Table 3-15. Critical Velocity for Full Pipe Conditions**

Average Velocity full pipe			3.25	ft/s	Critical Velocity (ft/s)		
Sim#	Free OH- Molar	Density (g/mL)	Na <sub>2</sub> U <sub>2</sub> O <sub>7</sub>				
			wt. %	vol. %	Poloski	Wilson & Judge	Max 30% margin
1	0.6	1.35	4.72	0.97	1.30	2.25	2.93
		1.33	4.49	0.91	1.36	2.27	2.95
		1.31	4.26	0.85	1.42	2.29	2.98
		1.27	3.77	0.73	1.47	2.33	3.03
	1.2	1.35	4.08	0.84	1.30	2.25	2.93
		1.33	3.86	0.78	1.36	2.28	2.96
		1.31	3.63	0.73	1.42	2.29	2.98
		1.27	3.16	0.62	1.54	2.33	3.04
2	0.6	1.25	1.30	0.25	1.48	2.36	3.07
		1.21	1.10	0.21	1.68	3.00	3.90
	1.2	1.25	1.09	0.21	1.52	2.65	3.45
		1.21	0.90	0.17	1.69	3.00	3.90

**Table 3-16. Slope for 75 gpm and Average Pipeline and Critical Velocities for Average Slope**

Sim#	Free OH <sup>-</sup> Molar	Density (g/mL)	Full Pipe Slope for 75 gpm ft <sub>vert</sub> /ft <sub>hori</sub>	Average Slope = 0.02232 ft <sub>vertical</sub> /ft <sub>horizontal</sub>			
				Average Pipeline Velocity (ft/s)	Critical Velocity (ft/s)		
					Poloski	Wilson & Judge	Max 30% margin
1	0.6 M	1.35	0.0172	4.22	1.42	2.46	3.20
		1.27	0.0164	4.31	1.46	2.54	3.31
	1.2 M	1.35	0.0173	4.22	1.42	2.46	3.20
		1.27	0.0164	4.31	1.61	2.55	3.31
2	0.6M	1.25	0.0181	4.14	1.62	2.58	3.36
		1.21	0.0168	4.27	1.84	3.28	4.26
	1.2M	1.25	0.0177	4.17	1.66	2.91	3.78
		1.21	0.0167	4.28	1.85	3.27	4.25

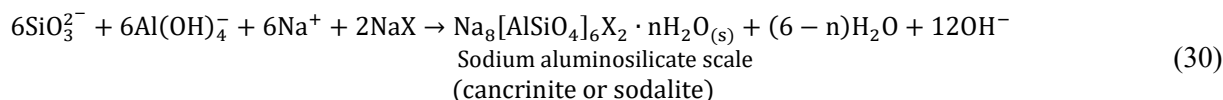
Based on the critical velocity calculations, any Simulant #1 condition can be processed. As for Simulant #2, the 1.25 g/mL can be processed, whereas the 1.21 case indicates settling could occur.

### 3.6 Literature Review and Modeling Regarding Formation of Aluminosilicates

#### 3.6.1 Literature Review

The formation of sodium aluminosilicate scale has long been recognized as an industrial-scale problem for the recovery cycle of Kraft pulp mills and during the Bayer process for aluminum production.<sup>33</sup> The scale is glossy and hard to remove once formed and may lower the efficiency of heat exchangers and the evaporation capacity of pulp mills. The scale formation becomes more severe in closed-cycle plant operation because the effluent is recycled, and the aluminum and silicon ion concentrations increase rapidly.

The Bayer process has been used to produce gibbsite from bauxite for over one hundred years. The aluminum-containing minerals in the bauxite ore are dissolved in hot sodium hydroxide solution as are quartz and kaolin, the two major silica contaminants. The dissolved silica precipitates as sodium aluminosilicate scale throughout alumina plants. The exact nature of the scale depends on the conditions of formation. The formation process can be written as equation (30):<sup>34</sup>



where X can be  $\frac{1}{2}\text{CO}_3^{2-}$ ,  $\frac{1}{2}\text{SO}_4^{2-}$ ,  $\text{Cl}^-$ , and  $\text{OH}^-$ .

Many investigations have been performed to evaluate the mechanisms for aluminosilicate formation and to identify means by which the formation process can be slowed or stopped. Gallop characterized naturally occurring aluminum-rich amorphous silica scales from geothermal brines to understand the formation mechanisms, and to investigate methods to inhibit their deposition.<sup>35</sup> Scale deposits examined in this study were formed by tetrahedrally-coordinated aluminum substitution within an amorphous silica framework. There was no evidence that aluminum in these scales derived from distinct aluminum minerals, such as gibbsite, or from aluminum silicate minerals transported in brine from the reservoir. The formation of aluminum-rich amorphous silica scale was dependent on brine pH, temperature, and aluminum concentration. Amorphous aluminum-rich silica was identified as a primary scale constituent deposited from certain geothermal brines. The scale was a non-stoichiometric compound exhibiting an empirical formula approaching  $\text{Al}_2\text{O}_3 \cdot (10-20)\text{SiO}_2$ , and consisted of aluminum incorporated in an amorphous silica matrix.

The effects of sodium carbonate concentration on both silica solubility and the crystallization of sodium aluminosilicates was investigated by Zheng et al. Isothermal batch precipitation experiments were performed using surrogate solutions based on the Bayer process to study this effect. At both 90 and 160 °C, cancrinite is the stable solid phase. Sodalite seed crystals transformed to cancrinite at both of these temperatures. A high concentration of sodium carbonate in the synthetic solutions caused a decrease in the rate of conversion of sodalite to cancrinite.<sup>34</sup>

Thermodynamic models have also been developed to calculate the solubility of aluminosilicates in aqueous alkaline solutions. Park and Englezos<sup>33</sup> developed a model which did not depend on parameters correlated from precipitation data in order to account for the effect of various ions on the aluminosilicate formation. The effects of  $\text{OH}^-$ ,  $\text{CO}_3^{2-}$ ,  $\text{SO}_4^{2-}$ ,  $\text{Cl}^-$ , and  $\text{HS}^-$  were considered using Pitzer's method to calculate activity coefficients. All parameters needed by the model were obtained from independent experimental data or available property estimation methods. The model calculated the molality of all species at equilibrium including the quantity of solid precipitates. The results were found to be sensitive to the value of the equilibrium constant for hydroxysodalite dihydrate formation and was generally in good agreement with experimental values.

The formation of aluminosilicate scale has also been identified as an issue with the liquid waste processing activities at the Savannah River Site (SRS). Aluminosilicate scale was observed in the 2H Evaporator in 1996 shortly after the startup of the Defense Waste Processing Facility (DWPF). The evaporator deposits resided on the evaporator wall and other exposed internal surfaces within the evaporator pot. Two solid nitrated aluminosilicate phases were identified which are known as (nitrated) cancrinite and sodalite. Both high-level liquid wastes (HLW) containing high concentrations of aluminum from the H-Canyon facility

and recycle water from the DWPF containing high concentrations of silicon were combined and evaporated to minimize the volume of space required for HLW storage. The crystallization of aluminosilicate scale (e.g., cancrinite and sodalite) in the evaporator that contained close to 10 wt% of enriched uranium ultimately led to the shutdown of the evaporator in October 1999. The scale was very similar to that observed in the aluminum and pulp and paper industries. Since the formation of solids in the evaporator resulted in the accumulation of fissile material, the scale deposition introduced criticality as well as operational concerns.<sup>36,37,38,39,40,41</sup> To understand the mechanisms associated with the formation of the aluminosilicate scale and to identify methods to reduce or eliminate its formation, a number of research studies were performed at the Savannah River Technology Center (SRTC) and by other research organizations.

Although the chemistry of the aluminosilicate scale formation in the 2H Evaporator was established, the mechanism(s) for deposition were not initially well understood. To address the scale formation, experiments were performed to determine if chemical agents could prevent the aluminosilicate formation.<sup>42</sup> The materials tested included: (1) divalent cations ( $Mg^{2+}$  or  $Ca^{2+}$ ), (2)  $KBF_4$  and fluoride, (3) ethylenediaminetetraacetic acid and derivatives, (4) Geosperse C-44 (crystal growth inhibitor), (5) Bis-Tris (buffering agent), and (6) LUDOX<sup>®</sup> inhibitor in Dowsil<sup>™</sup>. Results from these experiments indicated that the materials tested were not effective at limiting the formation of the thermodynamically stable aluminosilicates. Research in collaboration with the UNOCAL Corporation did show some reduction in the amount of aluminosilicate precipitation with three candidate materials (Geosperse C-44, Geogard, and Cridos 93P10); although, the inhibitors were not considered very effective in preventing precipitation.

The chemistry, crystallization, physicochemical properties, and behavior of sodium aluminosilicate solid phases were investigated through a collaborative partnership between the SRTC and the University of South Australia.<sup>43</sup> During this work, four sodium aluminosilicate precipitation products were synthesized which included: (1) an X-ray diffraction amorphous phase, (2) crystalline zeolite A, (3)  $NO_2/NO_3$ -rich crystalline sodalite, and (4)  $NO_2/NO_3$ -rich crystalline cancrinite. The characterization of the physicochemical properties for the four phases was performed under conditions simulating SRS liquid waste processing. Over a relatively short time frame, the rapidly occurring kinetic processes were found to dominate the crystallization behavior more strongly than the thermodynamics; however, over a long time period, the entire process behavior was governed by thermodynamics. Phase transformations involving amorphous, zeolite A, sodalite and cancrinite particles occurred by solution-mediated dissolution of the less stable phase and subsequent recrystallization of the more stable phase at different rates, all of which increase rapidly with increasing temperature. The equilibrium solubility of sodium aluminosilicate phases was highly dependent on the solid phase type, temperature, and the solution hydroxide, aluminum, nitrate and nitrite concentrations. The equilibrium solubility of all sodium aluminosilicate solid phases increased nonlinearly with increasing temperature and hydroxide concentration but decreased significantly with increasing aluminum concentration. The fouling of stainless-steel substrates using both unseeded and seeded systems was investigated. Seeding the solution (by adding sodium aluminosilicate crystals) tended to reduce the fouling as the rapidly growing crystals reduced the degree of supersaturation; although, fouling was observed in solutions with a low degree of supersaturation. The authors concluded that the fouling of the SRS 2H evaporator appeared to involve several parallel processes including initiation of sodium aluminosilicate nucleation, particle/crystal growth, transport of solution species and particles (bulk solution nuclei), particle attachment and removal, and scale layer growth.

To address the issue of the incorporation of uranium in the aluminosilicate scale which accumulated in the 2H evaporator, several studies were performed to determine possible causes. Batch experiments were conducted at Oak Ridge National Laboratory (ORNL)<sup>37</sup> in which simulated solutions were prepared and contacted with: (1) uranium solutions/precipitate slurries with sodium aluminosilicates on stainless steel surfaces, (2) uranium solutions with sodium aluminosilicate particles, and (3) precipitated uranium-containing particles with solutions containing aluminum and silicon. Results from these experiments

showed that uranium can be incorporated in sodium aluminosilicate solids through encapsulation in bulk agglomerated sodium aluminosilicate particles of different phases (amorphous, zeolite A, sodalite, and cancrinite) as well as through heterogeneous deposition on the surfaces of sodium aluminosilicate coatings (amorphous and cancrinite) grown on stainless steel. The results also indicated that sodium aluminosilicate particles can grow on the surfaces of precipitated uranium solids. Particularly notable for evaporator operations was the finding that uranium solids can form on existing sodium aluminosilicate scale, including cancrinite solids. If sodium aluminosilicate scale is present, and uranium is in sufficient concentration in solution to precipitate, a portion of the uranium can be expected to become associated with the scale. Under conditions of uranium compound precipitation in bulk solution, in the absence of sodium aluminosilicate, uranium phase precipitation did not occur on bare stainless-steel surfaces. The precipitation tests demonstrated that the mechanisms of uranium incorporation in the sodium aluminosilicate scale in the 2H evaporator could be either uranium–sodium aluminosilicate particle aggregation and encapsulation or surface growth/deposition of uranium on sodium aluminosilicate and/or surface growth/deposition of sodium aluminosilicate on uranium solid surfaces.

A research study was also performed to improve the fundamental understanding of the mechanisms of uranium accumulation with sodium aluminosilicates in evaporators and in other SRS process areas that may concentrate uranium in the presence of silicates.<sup>38,40</sup> The primary objective of this work was the use of X-ray absorption fine structure (XAFS) to obtain information on uranium speciation associated with sodium aluminosilicate solids that were synthesized with dissolved uranium. Results from these studies showed that the uranium uptake from solution was greater during the precipitation of sodalite and amorphous zeolite precursor material (i.e., reactive oxides, soluble silicates, and soluble aluminates in caustic solution which can combine to form a sodium aluminosilicate hydrogel at ambient temperature) than during the precipitation of zeolite A and amorphous zeolite. Mass balances for uranium in these materials indicate that during formation, the incorporation of uranium within these structures is not a likely mechanism for accumulation. However, uptake of uranium was greatest during the precipitation of amorphous zeolite precursor material. Additionally, removal of uranium from solution by surface sorption on the sodium aluminosilicate solids (a process which could have occurred after these solids were formed) probably had a minor role with respect to uranium accumulation in the 2H Evaporator. Processes most likely to have a large influence on uranium accumulation were uranium (VI) precipitation (as uranyl/uranate oxide/oxyhydroxides) and formation of an amorphous uranium-silica material.

In a second study, batch experiments were performed to evaluate incorporation of uranium into aluminosilicate structures during synthesis.<sup>39</sup> These experiments were designed to provide insight into the possibility of physically or chemically trapping uranium as solids in sodium aluminosilicate structures during synthesis in a supersaturated and highly caustic environment. However, conditions that favor the precipitation of aluminosilicates also promote the precipitation of uranium solids, so it was difficult to attribute problems with uranium accumulation to only the formation of the aluminosilicates. Infrared spectra of the precipitants showed that sodium uranates, uranium silicates, and other uranium solids were formed during the synthesis of sodium aluminate structures in the presence of uranium. Both amorphous and sodalite aluminosilicate phases, unlike the zeolite A phase, showed an appreciable affinity for uranium incorporation during their formation.

Thermodynamic models were developed for use as tools in predicting the formation of aluminosilicates in SRS evaporators and related tank waste (i.e., receipt tanks for the evaporators). A thermodynamic equilibrium model was developed at ORNL based on the code SOLGASMIX.<sup>44</sup> This thermodynamic model uses the Pitzer method to calculate activity coefficients, and many of the required Pitzer parameters were determined in the course of this work. The model simulated the phase equilibrium of SRS waste within the temperature range of 25-125 °C. The model was validated by comparing calculated solubilities to experimental data throughout this temperature range. The SOLGASMIX model was used to predict precipitations in SRS waste simulants at 25, 55, and 80 °C. The predictions were consistent with

measurements, although the calculated solubilities were slightly higher than the data. Predictions of aluminosilicate solubilities in  $\text{NaNO}_3$ - $\text{NaNO}_2$ - $\text{NaOH}$  solutions were consistent with kinetic data trends at 80 and 120 °C. The code calculations reflected decreasing aluminosilicate solubility with increasing temperature, consistent with all the data. Calculations performed using the GWB code were compared to the SOLGASMIX results and experimental solubilities. In some cases, the GWB results made poor predictions, due largely to the inadequacy of the B-dot model for activity coefficients.

Jantzen et al.<sup>36</sup> also performed extensive analysis and modeling of the formation of aluminosilicates in the 2H evaporator. Analysis of the deposits indicated that amorphous aluminate phase may be involved in causing the deposits to form and adhere to the evaporator wall. A possible mechanism for the evaporator scale formation was suggested based on the discovery of crystalline  $\text{Al}(\text{OH})_3$  adhering to the walls of (304-L stainless steel) waste tanks in the SRS M-Area. Reactive oxides, soluble silicates, and soluble aluminates in caustic solution can combine to form a sodium aluminosilicate hydrogel at ambient temperature when the solution stoichiometry of constituent aluminate and silicate species is approximately 1:1. The hydrogel converts to zeolite A under hydrothermal conditions at elevated temperature like conditions that exist in SRS evaporators. Nitrated-cancrinite/sodalite scale subsequently forms from the zeolite A. The sequential transformations of the sodium aluminosilicate hydrogel to the cancrinite/sodalite scale are densification (aging) transformations that require the saturation of the solution with respect to the hydrogel phase.

Modeling of the SRS evaporator feed and drop tank chemistries was performed using a commercially available software package, GWB. The GWB thermodynamic database is maintained by Lawrence Livermore National Laboratory. The database contains many radioactive and some metastable phases such as hydrogels, (e.g., precipitated  $\text{Fe}(\text{OH})_3$ ) which are pertinent to the relatively short kinetic regimes during which the evaporator deposits form. The database was augmented with: (1) solubility data for  $\text{NaAlO}_4$ ,  $\text{Al}(\text{OH})_3$ ,  $\text{AlOOH}$  developed at Hanford, (2) zeolite A and a sodium aluminosilicate gel ( $\text{NAS}_{\text{gel}}$ ) known to form in evaporators used for processing aluminum ore using the Bayer aluminum refining process, (3) “mixed zeolite” (a partially crystallized mixture of  $\text{NAS}_{\text{gel}}$  + zeolite A + cancrinite formed in evaporators used to process pulp and paper using the Kraft process, (4) hydroxysodalite data generated in support of the Kraft pulp and paper process, and (5)  $\text{NaNO}_3$ . The solubility of these phases as a function of temperature was entered into the database at a reference 8.5 molal sodium concentration pertinent to the evaporator solutions.<sup>36</sup> The calculational results from GWB were subsequently validated based on experimental work performed at the Pacific Northwest and Oak Ridge National Laboratories showing that GWB was an appropriate tool for use in SRS evaporator modeling and control.<sup>45</sup>

Jantzen et al.<sup>36</sup> explained the operational history of the 2H evaporator in terms of four different time populations based on operational records of the mass of silicon and aluminum sent to Tank 43H (i.e., the 2H Evaporator feed tank) from DWPF and H-Canyon:

- High silicon, low aluminum processing characterized by frequent large DWPF Slurry Mix Evaporator (SME) carryovers enriched in silicon-containing frit (January 1996-June 1997),
- Moderate silicon, low aluminum processing characterized by few SME carryovers, some without frit and little aluminum from H-Canyon (August 1997-March 1998),
- Moderate silicon, moderate aluminum processing characterized by few SME carryovers, some without frit and little aluminum from H-Canyon (April 1998-December 1998),
- High aluminum, moderate silicon processing characterized by no SME carryovers and high aluminum from H-Canyon (December 1998-October 1999).

The initial fouling of the 2H Evaporator with aluminosilicates was observed during a time when high silicon and low aluminum were processed. At this time, the feed location in Tank 43H was in close proximity to a zone (i.e., layer) in the tank enriched in silicon, iron, and uranium that exists above the sludge and the

DWPF recycle stream was overly enriched in silica due to uncontrolled SME carryovers which contained >50 wt% silica in the form of glass forming frit. The GWB modeling indicated that the evaporator feed was saturated with respect to the  $\text{NAS}_{\text{gel}}$  phase and  $\text{Na}_2\text{U}_2\text{O}_7$ . In addition, zeolite seed material was fed to the evaporator prior to the SME carryovers in the form of silica-rich residues from a large-scale High Efficiency Mist Eliminator (HEME)/High Efficiency Particulate Air (HEPA) filter dissolution demonstration at DWPF. As a result of these operations, the 2H Evaporator was fed high silicon-containing solutions that had zeolite seed crystals present to initiate fouling and scale deposition.<sup>36</sup>

Acceptable operation of the 2H Evaporator was obtained when moderate silicon and low aluminum feeds were used. A new feed pump was installed in Tank 43H which was well above the zone in the tank which was enriched in silicon, iron, and uranium. The DWPF recycle stream contained only a few SME carryovers and several of them did not contain glass forming frit. The GWB modeling showed that the evaporator feed was not saturated with respect to the  $\text{NAS}_{\text{gel}}$  phase, but was saturated with respect to  $\text{Na}_2\text{U}_2\text{O}_7$ .<sup>36</sup>

The second period of fouling of the 2H Evaporator initiated during the feeding of a stream containing moderate silicon and moderate aluminum. The position of the feed pump in Tank 43H remained unchanged and the DWPF recycle stream contained no SME carryovers. However, H-Canyon started to transfer wastes moderately high in aluminum. The GWB modeling showed that the evaporator feed was initially unsaturated with respect to the  $\text{NAS}_{\text{gel}}$  phase, but became saturated with respect to this phase when the aluminum concentration in the feed increased. The evaporator solutions were also saturated with respect to  $\text{Na}_2\text{U}_2\text{O}_7$  during the feeding of the moderate Al feed stream.<sup>36</sup>

An experimental study was also conducted to examine the fate of uranium during the formation of sodium aluminosilicates when wastes containing high aluminate concentrations were mixed with wastes of high silicate concentration.<sup>41</sup> The testing was conducted at varying degrees of uranium saturation using experimental conditions which were typical of SRS waste tanks (e.g., stagnant and slightly elevated temperature – 50 °C). The data showed that if the uranium concentration was above the solubility limit (i.e., the solution was supersaturated with uranium), the formation of sodium aluminosilicates can then act as a means to reduce the degree of supersaturation. The exact mechanism for the removal of the uranium from solution was not examined. Experimental results showed that under sub-saturated conditions, uranium was not removed from solution to any large extent in both simulant testing and actual tank waste testing. There were data supporting a small removal due to sorption of uranium on sites in the sodium aluminosilicates. At the solubility limit, it appears that uranium was not affected.

### *3.6.2 Summary of Literature Review Applied to Aluminosilicate Scale Formation during Neutralization*

The neutralization of ASNF in the H-Canyon facility combines the precursor materials which have the potential to form aluminosilicates in the processing tank, although not at the 1:1 aluminate:silicate ratio necessary for the formation of the sodium aluminosilicate hydrogel precursor discussed below. Sodium aluminosilicate scale has long been recognized as an industrial problem for the recovery cycle of Kraft pulp mills and during the Bayer process for aluminum production. The formation of aluminosilicate scale was also identified as an issue with the liquid waste processing activities at the SRS. Aluminosilicate scale was observed in the 2H Evaporator in 1996 shortly after the startup of the DWPF. Two solid nitrated aluminosilicate phases were identified which are known as (nitrated) cancrinite and sodalite.

To assist in understanding of the mechanisms which lead to the formation of aluminosilicates and to identify methods to reduce or eliminate their formation, a number of studies were performed at the SRTC and other research institutions. Over a relatively short time frame, the rapidly occurring kinetic processes were found to dominate the crystallization behavior of aluminosilicates more strongly than the thermodynamics; however, over a long time period, the entire process behavior was governed by thermodynamics. Phase transformations involving amorphous, zeolite A, sodalite and cancrinite particles occurred by solution-mediated dissolution of the less stable phase and subsequent recrystallization of the more stable phase at

different rates, all of which increase rapidly with increasing temperature. The equilibrium solubility of sodium aluminosilicate phases was highly dependent on the solid phase type, temperature, and the solution hydroxide, aluminum, nitrate and nitrite concentrations. The equilibrium solubility of all sodium aluminosilicate solid phases increased nonlinearly with increasing temperature and hydroxide concentration but decreased significantly with increasing aluminum concentration.

Extensive analysis and modeling of the formation of aluminosilicates in the 2H evaporator were performed. A possible mechanism for the evaporator scale formation was suggested based on the discovery of crystalline  $\text{Al}(\text{OH})_3$  adhering to the walls of waste tanks in the SRS M-Area. Reactive oxides, soluble silicates, and soluble aluminates in caustic solution can combine to form a sodium aluminosilicate hydrogel at ambient temperature when the solution stoichiometry of the aluminate and silicate species is approximately 1:1. The hydrogel converts to Zeolite-A under hydrothermal conditions at elevated temperature like conditions that exist in SRS evaporators. Nitrated-cancrinite/sodalite scale subsequently forms from the Zeolite-A. The sequential transformations of the sodium aluminosilicate hydrogel to the cancrinite/sodalite scale are densification (aging) transformations that require the saturation of the solution with respect to the hydrogel phase. It is very unlikely that the concentration of silicate species will ever approach the aluminate concentration following neutralization of ASNf. The total uranium concentration following fuel dissolution is less than 10 g/L (i.e., less than 0.042 M) compared to Al concentrations which are approximately 1.75 M.<sup>6</sup> For a uranium silicide fuel ( $\text{U}_3\text{Si}_2\text{-Al}$ ), the corresponding Si concentration would be less than 0.028 M. Therefore, based on the suggested mechanism, the sodium aluminosilicate hydrogel will never form which is a precursor to the Zeolite-A and subsequently the nitrated-cancrinite/sodalite scale.

Studies were also performed to address the issue of the incorporation of uranium in the aluminosilicate scale which accumulated in the 2H evaporator. Results from these studies showed that uranium can be incorporated in sodium aluminosilicate solids through encapsulation in bulk agglomerated sodium aluminosilicate particles of different phases (amorphous, zeolite A, sodalite, and cancrinite) as well as through heterogeneous deposition on the surfaces of sodium aluminosilicate coatings (amorphous and cancrinite) grown on stainless steel. However, uranium incorporation into the aluminosilicate structure is not a likely mechanism for accumulation. The results also indicated that sodium aluminosilicate particles can grow on the surfaces of precipitated uranium solids. If sodium aluminosilicate scale is present, and uranium is in sufficient concentration in solution to precipitate, a portion of the uranium can be expected to become associated with the scale. However, as stated above sodium aluminosilicate hydrogel will never form (due to the low silicate concentration) which is a precursor to the Zeolite-A and subsequently the nitrated-cancrinite/sodalite scale.

The modeling of the SRS evaporator feed and drop tank chemistry was performed using GWB, a commercially available software package. The calculational results from the GWB were validated based on experimental work performed at the Pacific Northwest and Oak Ridge National Laboratories. The GWB successfully predicted the saturation of the 2H evaporator feed with the sodium aluminosilicate hydrogel based on contents of the feed stream during the two periods where fouling occurred. The formation of the hydrogel is a prerequisite for scale formation as well as the hydrothermal conditions which exist in the evaporator. Therefore, results from using the GWB to model the neutralization of dissolved ASNf which predict the absence of the aluminosilicate hydrogel provides convincing evidence that scale would not form upon the solution neutralization.

Leaks from the neutralization tank containing solids which are re-acidified and dissolved prior to evaporation will not result in the formation of aluminosilicate scale during evaporation. Soluble Al will not co-precipitate with Si from an acidic solution. If the solution is high in silicon, there is potential to form silica solids during evaporation if the solubility limit is exceeded.

### 3.6.3 Results of GWB Modeling

The predicted mineral phases for the neutralization of Simulant #1 are shown in Figure 3-6. Since Si was not present in the simulant and is required for aluminosilicate formation, a bounding amount for a dissolver batch (400  $\mu\text{g/mL}$ ) was added for modeling purposes based on an evaluation of the capacity of the 10.3C centrifuge for Si removal.<sup>24</sup> The x-axis shows the amount of NaOH added in units of moles to the 1 L of starting acidic simulant. The final data point (9.83 mol NaOH added) is equivalent to 1.2 M free hydroxide. The y-axis shows the amount of solid precipitated in units of grams. The most prolific phase that formed was  $\text{Al}(\text{OH})_3$ , gibbsite, which reached a maximum mass of 115 g at approximately 6 moles of NaOH addition before slowly dissolving with increasing NaOH addition. At the end of the neutralization, greater than 99.999% of the initial U added was mineralized in the form of  $\text{Na}_2\text{U}_2\text{O}_7$ , sodium diuranate. Approximately 0.9 g of  $\text{Na}_2\text{Al}_2\text{Si}_3\text{O}_{10}\cdot 2\text{H}_2\text{O}$ , natrolite (a zeolite phase) was thermodynamically predicted to form with less than 7 moles of NaOH added and persisted through the end of the simulated neutralization.

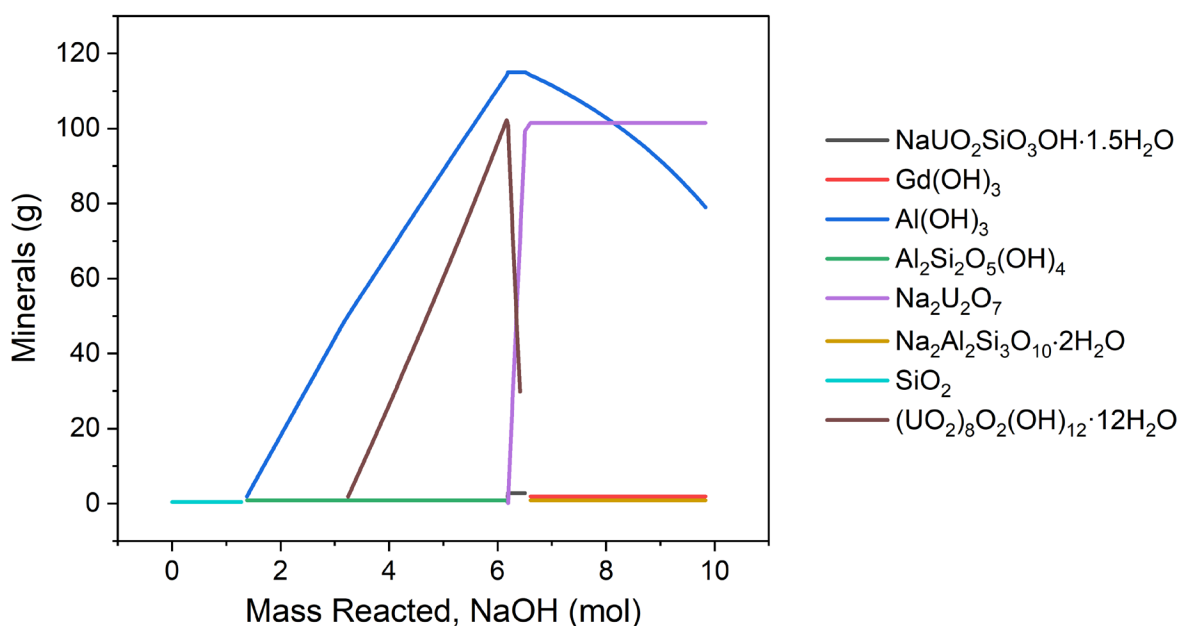


**Figure 3-6. The mineral phases that were predicted by GWB 12.0.5 to precipitate during the neutralization of Simulant #1.**

The predicted mineral phases for the neutralization of Simulant #2 (with the addition of Si based on the bounding concentration<sup>24</sup>) are shown in Figure 3-7. The most significant mineral phase formed during this simulated neutralization was FeO, ferrous oxide, which started to precipitate with the addition of approximately 4 moles of NaOH and reached a maximum mass of approximately 109 g during the simulation. Similar to Simulant #1, the final state of greater than 99.999% of the U in the system was in the mineral form  $\text{Na}_2\text{U}_2\text{O}_7$ . No zeolite mineral phases were observed to form in the model of Simulant #2. The Si was consumed in the daphnite-14A ( $\text{Fe}_5\text{Al}_2\text{Si}_3\text{O}_{10}(\text{OH})_8$ ) phase before any zeolites could form (i.e., the thermodynamics favored Si forming daphnite more so than zeolite).

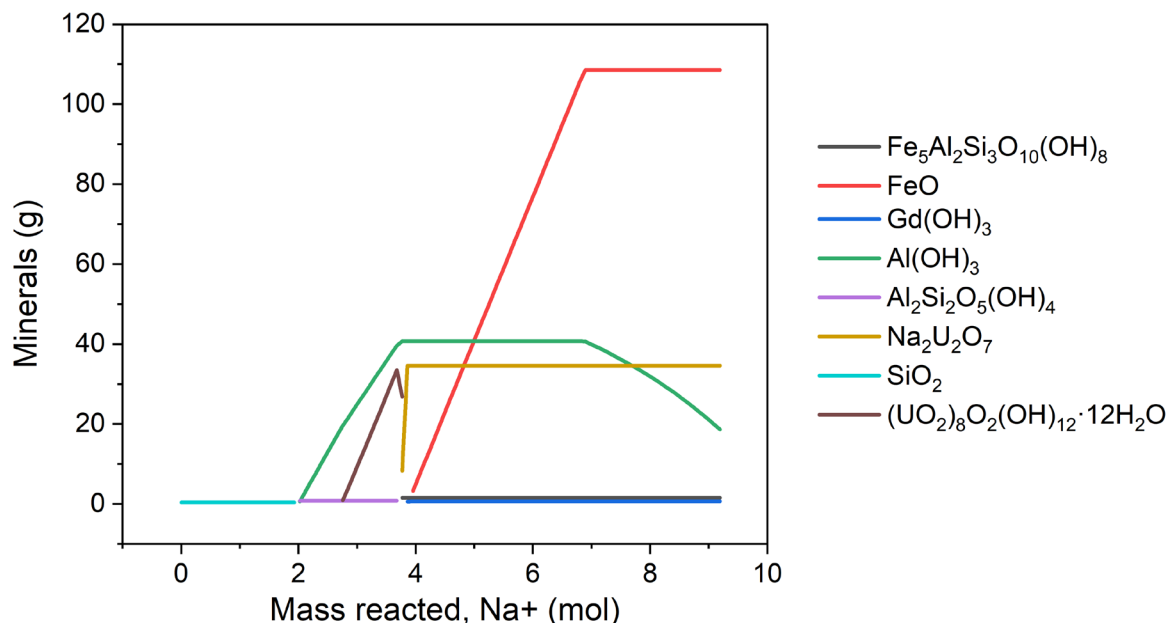


**Figure 3-7. The mineral phases that were predicted by GWB 12.0.5 to precipitate during the neutralization of Simulant #2.**

The mineral phases identified by the GWB in Figure 3-6 and Figure 3-7 from the modeling of the neutralization of the SNF simulants do not include the sodium aluminosilicate hydrogel which was identified as a precursor to the formation of scale in the 2H evaporator. Hydrogel formation may occur when the solution stoichiometry of the aluminate and silicate species is approximately 1:1, which does not occur even for the dissolution of uranium silicide fuels (see Section 3.6.2). The hydrogel converts to Zeolite-A under hydrothermal conditions at elevated temperature like conditions that exist in SRS evaporators (e.g., 120 °C) and subsequently to nitrated-cancrinite/sodalite scale. Therefore, in the absence of the hydrogel and the necessary hydrothermal conditions, it is highly unlikely that scale will form during the neutralization of SNF solutions in the H-Canyon neutralization tank.

## 4.0 Conclusions

Neutralizations were successfully completed on two different simulants of H-Canyon dissolver solution. The first simulant represented a batch of dissolver solution from dissolution of HFIR fuel after isotopic adjustment to 3 wt%  $^{235}\text{U}$  and poisoning with Gd at a ratio of 0.625:1 Gd: $^{235}\text{U}$ . The second simulant also represented a batch of dissolved HFIR fuel, adjusted to 3 wt%  $^{235}\text{U}$  enrichment, with Gd added at a ratio of 0.625:1, but also included the addition of Fe as a neutron poison at a ratio of 160:1 Fe: $^{239}\text{Pu}$  equivalent. Sodium hydroxide solution (50 wt%) was added to each simulant to reach the target endpoints of 0.6 M and 1.2 M free hydroxide. Analysis of samples taken throughout the neutralization indicated the lowest Gd: $^{235}\text{U}$  ratio was observed at about the mid-point of the neutralization where the ratio was 0.549 in the solids. This ratio is still well within the safety limits based on the NCSE performed previously.<sup>30</sup> Similar results were obtained for the simulant also containing Fe, where the minimum Gd: $^{235}\text{U}$  ratio observed was 0.552 in the solids.

Physical and rheological properties of the resulting neutralized simulants were also studied to provide the necessary data for performing flow calculations examining the transfer of neutralized slurry from H-Canyon to the CSTF. All endpoints had a final density above the 1.35 g/mL limit and therefore require further dilution at the end of the neutralization. For Simulant #1, it can be successfully transferred after dilution to a density between 1.27 and 1.35 g/mL for both the 0.6 M and 1.2 M  $\text{OH}^-$  endpoints. To minimize water

addition for Simulant #1, it is recommended to process at 1.35 g/mL. For Simulant #2, it was determined that flow will backup into the header if the pipe roughness is greater than 0.00015 ft for densities above 1.33 g/mL for the 0.6 M slurry. For Simulant #2 it is recommended to target final densities of 1.33 g/mL for the 0.6 M OH<sup>-</sup> endpoint or 1.35 g/mL for the 1.2 M OH<sup>-</sup> case if the transfer is non-Newtonian. If Simulant #2 is transferred as a Newtonian fluid, target 1.25 g/mL for either the 0.6 M or 1.2 M OH<sup>-</sup> endpoints, given densities higher than 1.25 g/mL should be treated as non-Newtonian. At 1.21 g/mL for Simulant #2, the critical velocity needed to maintain the Na<sub>2</sub>U<sub>2</sub>O<sub>7</sub> particles in suspension exceeds that of the pipeline velocity, indicating settling could occur. If there is excessive buildup in the piping from previous transfers (e.g., pipe roughness greater than 0.00125 ft), backup into the 10" header will occur for either simulant. Flushing after transfers is recommended at or above 75 gpm.

The literature survey identified numerous reports and studies related to the formation of sodium aluminosilicate scale both in the Kraft pulp mill and Bayer process for aluminum production in industry as well as in HLW processing activities at SRS. Formation of aluminosilicate scale has previously been identified as an issue in the liquid waste processing activities at SRS, particularly in the evaporators where HLW containing high concentrations of Al and recycle water from DWPF containing high concentrations of Si are combined and evaporated. Based on the proposed mechanism for the formation of the evaporator scale requiring a near 1:1 ratio of aluminate and silicate species for the formation of the sodium aluminosilicate hydrogel, it is unlikely to occur in the H-Canyon processes where the aluminate concentration will greatly exceed the silicate concentration. The total uranium concentration following fuel dissolution is less than 10 g/L (i.e., less than 0.042 M) compared to Al concentrations which are approximately 1.75 M.<sup>6</sup> For a uranium silicide fuel (U<sub>3</sub>Si<sub>2</sub>-Al), the corresponding Si concentration would be less than 0.028 M. This in combination with the lower temperatures in the neutralization tanks indicate that the formation of sodium aluminosilicate scale will not occur in H-Canyon. The neutralization reactions studied here were also modeled using GWB to identify the potential formation of sodium aluminosilicates in these streams. Modeling of the neutralization of Simulant #1 showed the Si present (based on a bounding concentration) precipitated in the form of a small amount of a sodium aluminosilicate phase (natrolite, Na<sub>2</sub>Al<sub>2</sub>Si<sub>2</sub>O<sub>10</sub>·2H<sub>2</sub>O) that formed just after the equivalence point of the neutralization was reached and persisted through the end of the simulated neutralization. The modeling also indicated that >99.999% of the initial U added was precipitated in the form of sodium diurate (Na<sub>2</sub>U<sub>2</sub>O<sub>7</sub>). In the case of Simulant #2, no zeolite mineral phases were observed to form, and again >99.999% of the U in the system was present as Na<sub>2</sub>U<sub>2</sub>O<sub>7</sub> at the end of the neutralization.

## 5.0 Future Work

Additional work may be necessary if the planned neutralizations/batches fall outside of the parameters tested here. Specifically, if the concentration of solids is expected to be higher than tested, additional calculations and/or experiments may be necessary to ensure the neutralized material can be successfully transferred.

## 6.0 References

- <sup>1</sup> Saldivar, E. and Watson, H., “Savannah River Accelerated Basin Deinventory”, SRNS-RP-2019-00651, Rev. 0, Savannah River Site, Aiken, SC, 2019.
- <sup>2</sup> W. E. Daniel, T. S. Rudisill, P. E. O’Rourke, and N. S. Karay, “Dissolution Flowsheet for High Flux Isotope Reactor Fuel”, SRNL-STI-2016-00485, Rev. 1, December 2017.
- <sup>3</sup> W. E. Daniel, T. S. Rudisill, and P. E. O’Rourke, “Dissolution of Material Test Reactor Fuel in an H-Canyon Dissolver”, SRNL-STI-2016-00725, Rev. 1, May 2018.
- <sup>4</sup> J. Benedict, “Waste Acceptance Criteria for Liquid Waste Transfers to the Tank Farms (U)”, X-SD-G-00009, Rev. 8, June 2021.
- <sup>5</sup> T. E. Smith, W. H. Clifton, “Inventory of Aluminum Spent Nuclear Fuel Evaluation”, SRNS-E1122-2020-00008, Rev. 0, November 11, 2020.
- <sup>6</sup> N. C. Fee, “Process Flow Diagram for Post-Accelerated Basin De-Inventory Initiative Implementation Canyon Processing”, SRNS-RP-2021-00062, Rev. 0, January 25, 2021.
- <sup>7</sup> T. E. Smith, “Neutralization of ABD Material”, NMMD-HTS-2021-3474, Rev. 0, March 2021.
- <sup>8</sup> Email from Bill Clifton to Tracy Rudisill on 5/6/21, documented in SRNL Electronic Laboratory Notebook #E7518-00472-03.
- <sup>9</sup> W. C. Horton and J. S. Willison, “Nuclear Criticality Safety Evaluation: Processing at DWPF (U)”, N-NCS-S-00012, Rev. 2, April 2021.
- <sup>10</sup> “Neutralizing High Activity Waste in Tank 8.4”, Procedure 221-H-4710, Rev. 62, February 4, 2021.
- <sup>11</sup> G. Akerlof and G. Kegeles, “The Density of Aqueous Solutions of Sodium Hydroxide”, *Journal of American Chemical Society*, 1939, 61, 5, pg. 1027-1032.
- <sup>12</sup> R.M. Felder and R.W. Rousseau, “Elementary Principles of Chemical Processing”, 3<sup>rd</sup> Edition, John Wiley & Sons, Inc., 2005.
- <sup>13</sup> R. Darby, “Chemical Engineering Fluid Mechanics”, 2<sup>nd</sup> Edition, Marcel Dekker, Inc. 2001.
- <sup>14</sup> Crane, “Flow of Fluids Through Valves, Fittings, and Pipe”, Technical Paper No. 410, 1988.
- <sup>15</sup> J.M. Pareizs, “Rheology and Flow Evaluation of Neutralized Sodium Reactor Experiment Fuel with Manganous Nitrate”, SRNL-STI-2020-00299, Rev. 0, October 2020.
- <sup>16</sup> R. W. Hanks, “The Laminar-Turbulent Transition for Fluids with a Yield Stress”, *American Institute Chemical Engineering Journal*, 1963, 9, 3, pg. 306-309.
- <sup>17</sup> ESDU 91025, “Non-Newtonian Fluids: Frictional Pressure Loss Predictions for Fully-Developed Flow in Straight Pipe”, October 1991.
- <sup>18</sup> A. R. Oroskar and R. M. Turian, “The Critical Velocity in Pipeline Flow of Slurries”, *AIChE*, Vol. 26, No. 4, July 1980
- <sup>19</sup> K.P. Recknagle and Y. Onishi, “Transport of Tank 241-SY-101 Waste Slurry: Effects of Dilution and Temperature on Critical Pipeline Velocity”, PNNL-12217, May 1999
- <sup>20</sup> A. P. Poloski and et al., “A Pipeline Transport Correlation for Slurries with Small but Dense Particles”, Vol. 88, pp. 182 -189, *The Canadian Journal of Chemical Engineering*, April 2010
- <sup>21</sup> A. P. Poloski and et al., “Deposition Velocities of Newtonian and Non-Newtonian Slurries in Pipelines”, PNNL-17639, Rev. 0, March 2009
- <sup>22</sup> T. Motyka, “Estimating the Floc Size and Concentration of Waste Slurries for use in Determining Transport Conditions for Inter-Area Transfers”, DPST-81-324, March 16, 1981
- <sup>23</sup> Heastad Press, “Computer Application in Hydraulic Engineering”, 7<sup>th</sup> Edition, 2002
- <sup>24</sup> T. S. Rudisill, “Removal of Silica from Dissolver Solutions by the 10.3C Centrifuge Following a Gelatin Strike”, SRNL-L3100-2014-00235, Rev. 0, October 2, 2014.
- <sup>25</sup> “Savannah River National Laboratory Technical Report Design Check Guidelines” WSRC-IM-2002-00011, Rev. 2, August 2004.
- <sup>26</sup> K. M. L. Taylor-Pashow, E. K. Hansen, and T. S. Rudisill, “Task Technical and Quality Assurance Plan for the Neutralization of Accelerated Basin De-inventory (ABD) Material”, SRNL-RP-2021-03800, Rev. 0, June 2021.

- 
- <sup>27</sup> Savannah River Site Manual E7 “Conduct of Engineering”, Procedure 2.60 Rev. 20 “Technical Reviews”, November 9, 2021.
- <sup>28</sup> SRNL Electronic Laboratory Notebook #E7518-00472-03.
- <sup>29</sup> A. C. Vermeulen, J. W. Geus, R. J. Stol, and P. L. De Bruyn, “Hydrolysis-Precipitation Studies of Aluminum(III) Solutions I. Titration of Acidified Aluminum Nitrate Solutions”, *J. Colloid and Interface Science*, **1975**, *51*, 449-458.
- <sup>30</sup> N. Devine and J. Butler, “Nuclear Criticality Safety Evaluation: Minimum Safe Gadolinium to Uranium Ratio in an Infinite System”, N-NCS-00326, Rev. 0, June 2020.
- <sup>31</sup> M. G. Bronikowski and T. S. Rudisill, “Neutralization of Plutonium and Enriched Uranium Solutions Containing Gadolinium as a Neutron Poison”, WSRC-TR-2004-00053, February 2004.
- <sup>32</sup> “Hot and Warm Canyon Process Piping and Equipment Scroll General Notes & Legend (U)”, S5-2-14421, Rev. 7, 1986.
- <sup>33</sup> H. Park and P. Englezos, “Thermodynamic Modeling of Sodium Aluminosilicate Formation in Aqueous Alkaline Solutions”, *Ind. Eng. Chem. Res.*, Vol. 38, pp. 4959-4965 (1999).
- <sup>34</sup> K. Zheng, A. R. Gerson, J. Addai-Mensah, R. St.C. Smart, “The influence of sodium carbonate on sodium aluminosilicate crystallisation and solubility in sodium aluminate solutions”, *Journal of Crystal Growth* Vol 171 pp. 197-208 (1997).
- <sup>35</sup> D. L. Gallup, “Aluminum Silicate Scale Formation and Inhibition: Scale Characterization and Laboratory Experiments”, *Geothermics*, Vol. 26, No. 4, pp. 483-499 (1997).
- <sup>36</sup> C. M. Jantzen, J. E. Laurinat, and K. G. Brown, “Thermodynamic Modeling of the SRS Evaporators: Part I. The 2H and 2F Systems”, WSRC-TR-2000-00293, Rev. 1, Savannah River Technology Center, Aiken, SC, April 4, 2002.
- <sup>37</sup> M. Z. Hu, D. W. DePaoli, and C. H. Mattus, “Uranium and Aluminosilicate Surface Precipitation Tests”, RNL/TM-2002/201, Oak Ridge National Laboratory, Oak Ridge, TN, November 2002.
- <sup>38</sup> M. C. Duff, D. B. Hunter, and L. N. Oji, “Characterization of Uranium Solids Precipitated with Aluminosilicates”, WSRC-TR-2002-00510, Savannah River Technology Center, Aiken, SC, November 26, 2002.
- <sup>39</sup> L. N. Oji & A. L. Williams, “Evaluation of Uranium Coprecipitation with Sodium Aluminosilicate Phases”, *Nuclear Technology*, Vol 145, pp. 215-229, 2003.
- <sup>40</sup> M. C. Duff, D. B. Hunter, L. N. Oji, and W. R. Wilmarth, “Characterization of Uranium Solids Precipitated with Aluminosilicates”, Waste Management 2004 Conference, Tucson, AZ, February 29 – March 4, 2004.
- <sup>41</sup> W. R. Wilmarth, J. T. Mills, V. H. Dukes, and R. C. Sullivan, “Fate of Uranium during Sodium Aluminosilicate Formation Under Waste Tank Conditions”, WSRC-TR-2005-00412, Savannah River National Laboratory, Aiken, SC, June 22, 2005.
- <sup>42</sup> W. R. Wilmarth and J. T. Mills, “Results of Aluminosilicate Inhibitor Testing”, WSRC-TR-2001-00230, Savannah River Technology Center, Aiken, SC, 2001.
- <sup>43</sup> J. Addai-Mensah, J. Li, M. Zbik, and S. Rosencrance, “The Chemistry, Crystallization, Physicochemical Properties and Behavior of Sodium Aluminosilicate Solid Phases: Final Report”, WSRC-MS-2002-00907, Savannah River Technology Center, Aiken, SC, November 20, 2002.
- <sup>44</sup> C. F. Weber, “Thermodynamic Modeling of Savannah River Evaporators”, ORNL/TM-2001/102, Oak Ridge National Laboratory, Oak Ridge, TN, August 2001.
- <sup>45</sup> J. M. Pareizs and C. M. Jantzen, “Thermodynamic Modeling of the SRS Evaporators: Part V. Validation”, WSRC-TR-2002-00331, Savannah River Technology Center, Aiken, SC, April 15, 2003.

**Appendix A. Elevation, Piping, and Fittings for H-Canyon Gravity Drain Lines to HPP 5 and HPP 6**



REVISION	DATE	BY	CHKD	APPD
1	10/1/78	W	W	W
2	10/1/78	W	W	W
3	10/1/78	W	W	W
4	10/1/78	W	W	W
5	10/1/78	W	W	W
6	10/1/78	W	W	W
7	10/1/78	W	W	W

REVISION	DATE	BY	CHKD	APPD
1	10/1/78	W	W	W
2	10/1/78	W	W	W
3	10/1/78	W	W	W
4	10/1/78	W	W	W
5	10/1/78	W	W	W
6	10/1/78	W	W	W
7	10/1/78	W	W	W

REVISION	DATE	BY	CHKD	APPD
1	10/1/78	W	W	W
2	10/1/78	W	W	W
3	10/1/78	W	W	W
4	10/1/78	W	W	W
5	10/1/78	W	W	W
6	10/1/78	W	W	W
7	10/1/78	W	W	W

REVISION	DATE	BY	CHKD	APPD
1	10/1/78	W	W	W
2	10/1/78	W	W	W
3	10/1/78	W	W	W
4	10/1/78	W	W	W
5	10/1/78	W	W	W
6	10/1/78	W	W	W
7	10/1/78	W	W	W

REVISION	DATE	BY	CHKD	APPD
1	10/1/78	W	W	W
2	10/1/78	W	W	W
3	10/1/78	W	W	W
4	10/1/78	W	W	W
5	10/1/78	W	W	W
6	10/1/78	W	W	W
7	10/1/78	W	W	W

REVISION	DATE	BY	CHKD	APPD
1	10/1/78	W	W	W
2	10/1/78	W	W	W
3	10/1/78	W	W	W
4	10/1/78	W	W	W
5	10/1/78	W	W	W
6	10/1/78	W	W	W
7	10/1/78	W	W	W

NOTE:  
1-W.P. EL. LOCATED AT 6' OF JACKET  
2-ALL ANGLES 90° UNLESS OTHERWISE NOTED

Q NOTES:  
WASTE PIPING JACKETS  
ARE CLASSIFIED AS  
BE PROJECT DAPP FOR  
DIA ACTION REQUIREMENTS

REVISION	DATE	BY	CHKD	APPD
1	10/1/78	W	W	W
2	10/1/78	W	W	W
3	10/1/78	W	W	W
4	10/1/78	W	W	W
5	10/1/78	W	W	W
6	10/1/78	W	W	W
7	10/1/78	W	W	W

REVISION	DATE	BY	CHKD	APPD
1	10/1/78	W	W	W
2	10/1/78	W	W	W
3	10/1/78	W	W	W
4	10/1/78	W	W	W
5	10/1/78	W	W	W
6	10/1/78	W	W	W
7	10/1/78	W	W	W

LEGEND

- A - PIPE ANCHOR FOR JACKET & CORES
- JS - JACKET SUPPORT
- CPS - CORE PIPE SUPPORT (NO HORIZ. RESTRAINT)
- S - SPACER FOR CORE PIPES IN JACKET
- G - JACKET GUIDE

STRESS CALCULATIONS REVISED

THIS DWG. CONTAINS LINES  
W/1100 & W/1101 FROM W/221H  
TO BEPP'S & HPP'S  
FOR PRG ELEV SEE W/1101D

REVISION	DATE	BY	CHKD	APPD
1	10/1/78	W	W	W
2	10/1/78	W	W	W
3	10/1/78	W	W	W
4	10/1/78	W	W	W
5	10/1/78	W	W	W
6	10/1/78	W	W	W
7	10/1/78	W	W	W

REVISION	DATE	BY	CHKD	APPD
1	10/1/78	W	W	W
2	10/1/78	W	W	W
3	10/1/78	W	W	W
4	10/1/78	W	W	W
5	10/1/78	W	W	W
6	10/1/78	W	W	W
7	10/1/78	W	W	W

REVISION	DATE	BY	CHKD	APPD
1	10/1/78	W	W	W
2	10/1/78	W	W	W
3	10/1/78	W	W	W
4	10/1/78	W	W	W
5	10/1/78	W	W	W
6	10/1/78	W	W	W
7	10/1/78	W	W	W

REVISION	DATE	BY	CHKD	APPD
1	10/1/78	W	W	W
2	10/1/78	W	W	W
3	10/1/78	W	W	W
4	10/1/78	W	W	W
5	10/1/78	W	W	W
6	10/1/78	W	W	W
7	10/1/78	W	W	W

REVISION	DATE	BY	CHKD	APPD
1	10/1/78	W	W	W
2	10/1/78	W	W	W
3	10/1/78	W	W	W
4	10/1/78	W	W	W
5	10/1/78	W	W	W
6	10/1/78	W	W	W
7	10/1/78	W	W	W

REVISION	DATE	BY	CHKD	APPD
1	10/1/78	W	W	W
2	10/1/78	W	W	W
3	10/1/78	W	W	W
4	10/1/78	W	W	W
5	10/1/78	W	W	W
6	10/1/78	W	W	W
7	10/1/78	W	W	W

REVISION	DATE	BY	CHKD	APPD
1	10/1/78	W	W	W
2	10/1/78	W	W	W
3	10/1/78	W	W	W
4	10/1/78	W	W	W
5	10/1/78	W	W	W
6	10/1/78	W	W	W
7	10/1/78	W	W	W

REVISION	DATE	BY	CHKD	APPD
1	10/1/78	W	W	W
2	10/1/78	W	W	W
3	10/1/78	W	W	W
4	10/1/78	W	W	W
5	10/1/78	W	W	W
6	10/1/78	W	W	W
7	10/1/78	W	W	W

REVISION	DATE	BY	CHKD	APPD
1	10/1/78	W	W	W
2	10/1/78	W	W	W
3	10/1/78	W	W	W
4	10/1/78	W	W	W
5	10/1/78	W	W	W
6	10/1/78	W	W	W
7	10/1/78	W	W	W

➡ ANALYZE FOR SAFETY, ECOLOGY, AND MINIMUM ESSENTIAL DESIGN ➡

**REQUIRED PIPING FLEXIBILITY DATA**

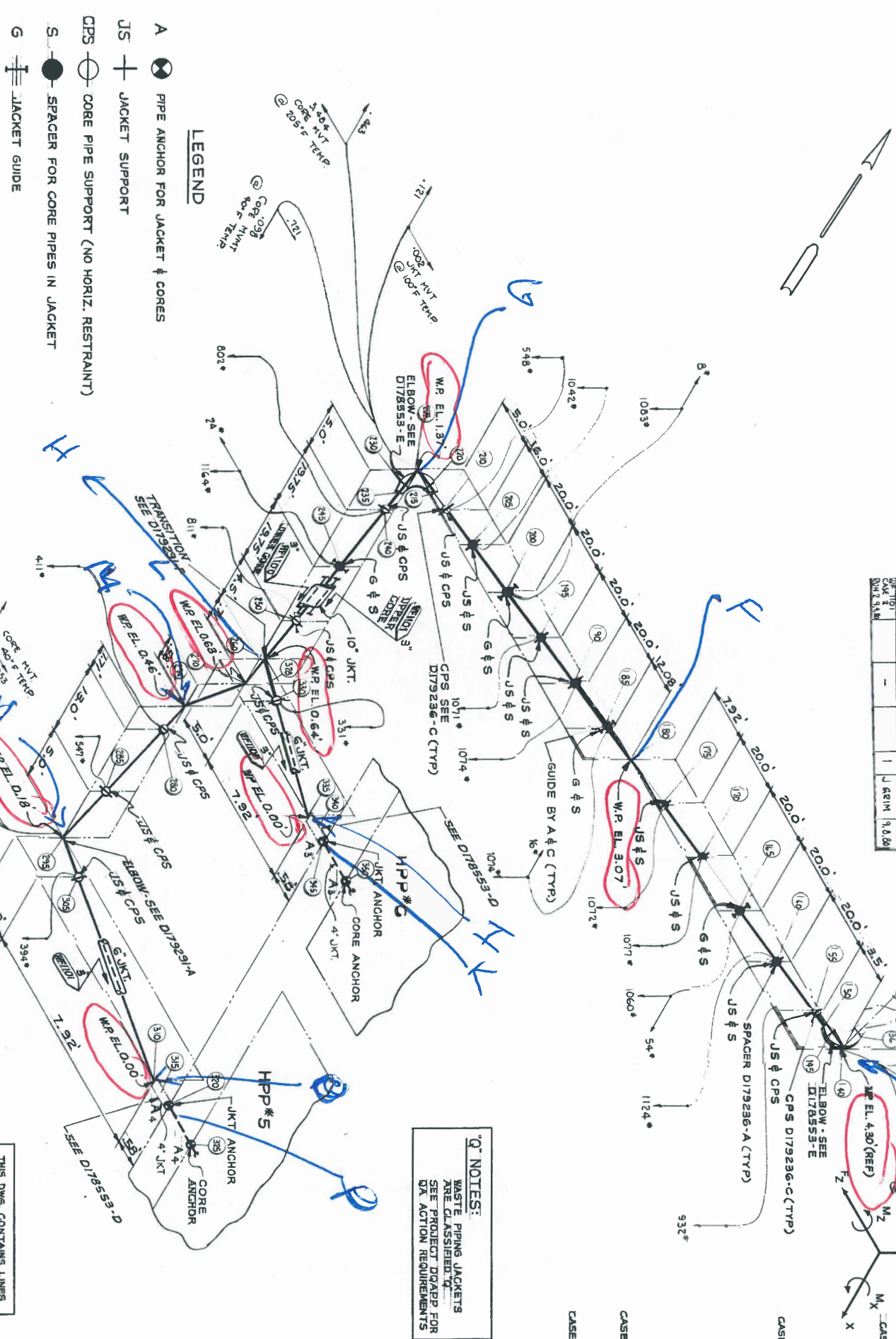
LINE NO.	PIPE	INSULATION	FLANGE	MEDIA						
				SP. GR.	MAX. PRESS. PSIG	MAX. OPER. TEMP °F	MAX. TEMP °F			
WJ010	P-1	SIZE SCH.	MATL.	THK. WT./FT.	TYPE	RATING				
	CODE									
WJ010	P45	3	40S 904L	—	—		1.5	150	176	235
WJ011	P45	3	40S 904L	—	—		1.5	150	176	235
JCT1	P51	10	20 C.S.	—	—	SSULINATE500	—	—	—	—
JCT2	P51	10	20 C.S.	—	—	—	—	—	—	—
JCT3	P51	10	C.S.	—	—	—	—	—	—	—
JCT4	P51	4	40 C.S.	—	—	—	—	—	—	—
JCT5	P51	4	40 C.S.	—	—	—	—	—	—	—
JCT6	P51	4	40 C.S.	—	—	—	—	—	—	—
JCT7	P51	4	40 C.S.	—	—	—	—	—	—	—
WJ017	P45	3	40S 904L	—	—		1.5	150	40	43
WJ018	P45	3	40S 904L	—	—		1.5	150	40	43
JCT1	P51	10	20 C.S.	—	—	SSULINATE 500	—	—	—	—
JCT2	P51	10	20 C.S.	—	—	—	—	—	—	—
JCT3	P51	10	C.S.	—	—	—	—	—	—	—
JCT4	P51	4	40 C.S.	—	—	—	—	—	—	—
JCT5	P51	4	40 C.S.	—	—	—	—	—	—	—
JCT6	P51	4	40 C.S.	—	—	—	—	—	—	—
JCT7	P51	4	40 C.S.	—	—	—	—	—	—	—






PIPING REACTIONS			FORCE LBS. MOMENTS FT.-LBS.	
FY	FZ	MX	MY	MZ

A 3	3551 3550	40	-281	-2342	4556	316	-3
A 4	3504 3525	76	-239	-2306	350	835	-41
A 3	345 f 3550	-23	-278	-2335	444	-222	16
A 4	320 f 325	-11	-236	-2362	525	117	-38

ANCHOR LOADS INCLUDE EFFECT OF GILSULATE 500 FORCE (100 # / SQ. FT.)  
INSTRUCTIONS FOR SKETCHING

**"Q" NOTES:**  
WASTE PIPING JACKETS  
ARE CLASSIFIED "Q."  
SEE PROJECT DQAPP FOR  
QA ACTION REQUIREMENTS



- A  PIPE ANCHOR FOR JACKET  $\nabla$  CORES
- JS  JACKET SUPPORT
- CPS  CORE PIPE SUPPORT (NO HORIZ. RESTRAINT)
- S  SPACER FOR CORE PIPES IN JACKET
- G  JACKET GUIDE

	DATA POINT	MAX STRESS SE	ALLOW STRESS SA	STRESS RSL	CYCLE LIFE
JACKET	245	1,186	30,000		+100,000
CORE LINE 2W1100	160	6,200	21,300		+100,000
CORE LINE 2W1101	160	6,120	21,300		+100,000

THIS DWS. CONTAINS LINES  
WF1100 & WF1101 FROM  
WF2214 TO HPP\*5 & HPP\*6  
FOR PP6 ELEV SEE W711910

\* DA  
 Y 510  
 Y 526  
 X 521  
 RMD REVIEWED  
 AT REV. 8/19/97  
 DATE 8/19/97

LAST				
REV.				
Q				
M/F	BLDG./PROJ.	DA	TYPE	
	241H 981965	*	29	W 712649

SAVANNAH RIVER PLANT  
BLDG. 241H REPLACE WASTE HDR.  
BLDG. 241H 981965

THIS DOCUMENT CONTAINS INFORMATION RELATING TO ACTIVITIES OF THE U.S. DEPARTMENT OF ENERGY. NOT TO BE REPRODUCED OR RELEASED WITHOUT PRIOR APPROVAL.

**PIPING FLEXIBILITY ANALYSIS**

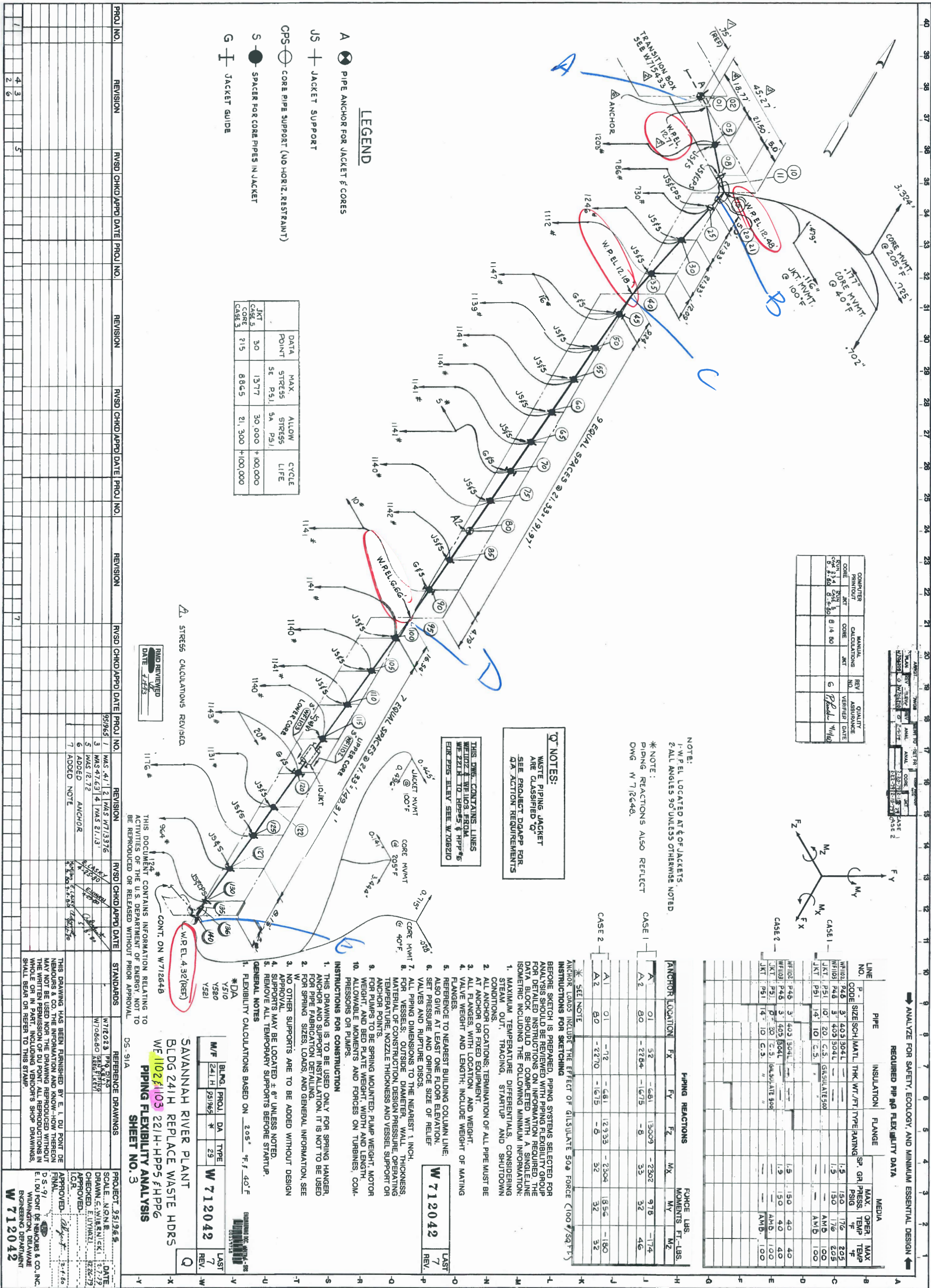
**SHEET NO.2**

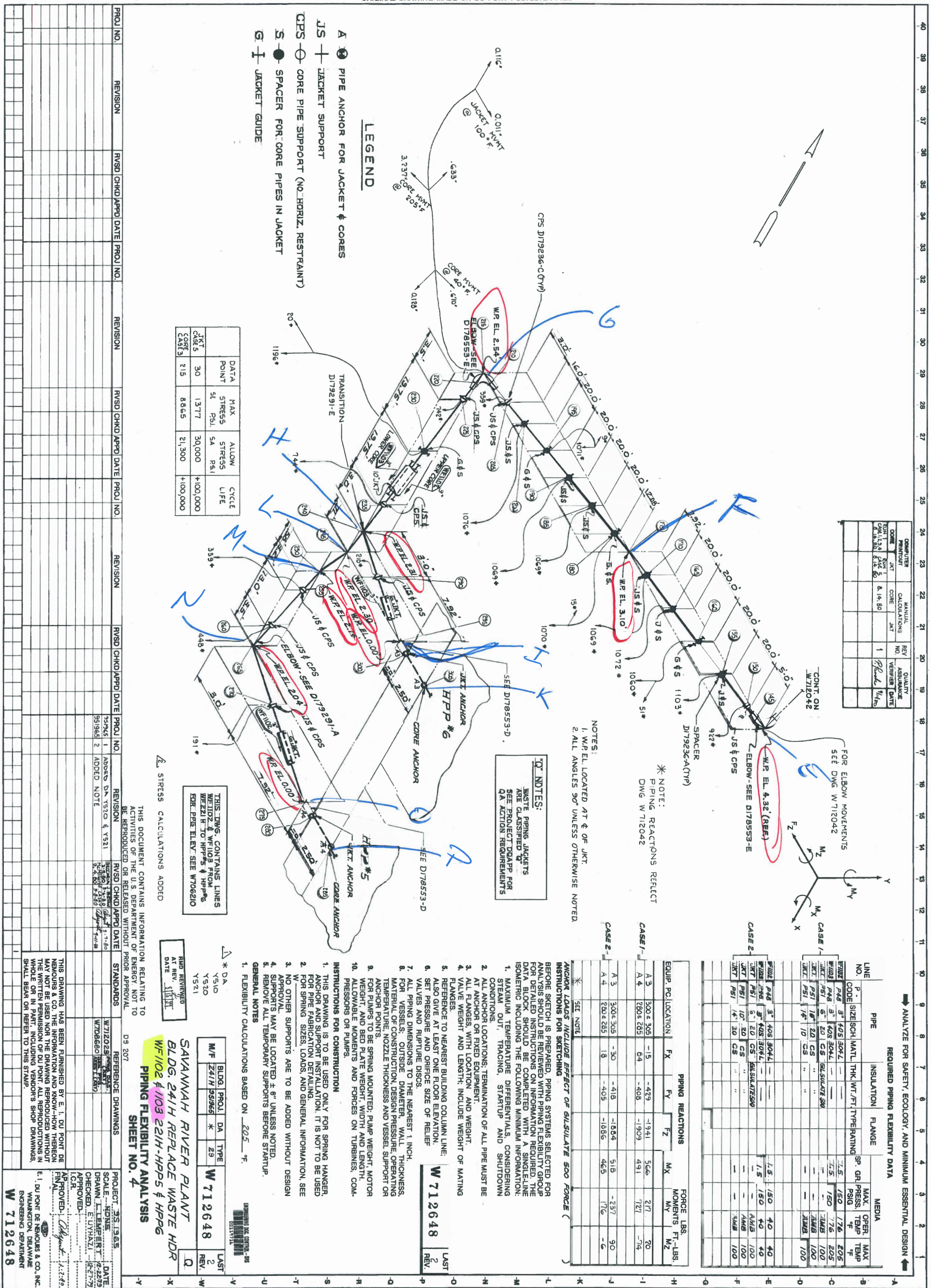
ANALYSIS BY JCO

REFERENCE NUMBER \_\_\_\_\_

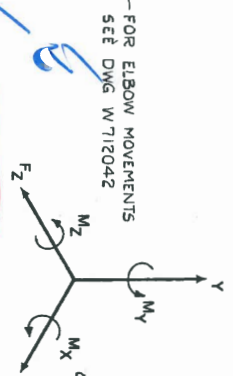
PROJ. NO.	REVISION	RVS'D	CHNGD	APPR'D	DATE	PROJ. NO.	REVISION	RVS'D	CHNGD	APPR'D	DATE	PROJ. NO.	REVISION	RVS'D	CHNGD	APPR'D	DATE	STAMP/STATUS
REFERENCE DRAWINGS																		
PROJECT: 392 19/65																		
DRAWING: 19/65-100																		

[illegible]





COMPUTER	MANUAL	REV	QUALITY
NO. 1	NO. 1	NO. 1	NO. 1
DATE	DATE	DATE	DATE
10/1/80	10/1/80	10/1/80	10/1/80



LINE NO.	PIPE	INSULATION	FLANGE	SP. GR. PRESS.	MAX. OPER. TEMP.
1	3" 40S 304L	---	---	---	---
2	3" 40S 304L	---	---	---	---
3	3" 40S 304L	---	---	---	---
4	3" 40S 304L	---	---	---	---
5	3" 40S 304L	---	---	---	---
6	3" 40S 304L	---	---	---	---
7	3" 40S 304L	---	---	---	---
8	3" 40S 304L	---	---	---	---
9	3" 40S 304L	---	---	---	---
10	3" 40S 304L	---	---	---	---
11	3" 40S 304L	---	---	---	---
12	3" 40S 304L	---	---	---	---
13	3" 40S 304L	---	---	---	---
14	3" 40S 304L	---	---	---	---
15	3" 40S 304L	---	---	---	---
16	3" 40S 304L	---	---	---	---
17	3" 40S 304L	---	---	---	---
18	3" 40S 304L	---	---	---	---
19	3" 40S 304L	---	---	---	---
20	3" 40S 304L	---	---	---	---
21	3" 40S 304L	---	---	---	---
22	3" 40S 304L	---	---	---	---
23	3" 40S 304L	---	---	---	---
24	3" 40S 304L	---	---	---	---
25	3" 40S 304L	---	---	---	---
26	3" 40S 304L	---	---	---	---
27	3" 40S 304L	---	---	---	---
28	3" 40S 304L	---	---	---	---
29	3" 40S 304L	---	---	---	---
30	3" 40S 304L	---	---	---	---
31	3" 40S 304L	---	---	---	---
32	3" 40S 304L	---	---	---	---
33	3" 40S 304L	---	---	---	---
34	3" 40S 304L	---	---	---	---
35	3" 40S 304L	---	---	---	---
36	3" 40S 304L	---	---	---	---
37	3" 40S 304L	---	---	---	---
38	3" 40S 304L	---	---	---	---
39	3" 40S 304L	---	---	---	---
40	3" 40S 304L	---	---	---	---

EQUIP. PC. LOCATION	FX	FY	FZ	MX	MY	MZ
A 3	300	305	-15	-429	-1941	506
A 4	280	205	64	-408	-1909	491
A 3	300	305	-30	-418	-1884	518
A 4	280	205	18	-405	-1886	465

ANCHOR LOADS INCLUDE EFFECT OF ISOLATE 500 FORCE ( )

INSTRUCTIONS FOR SKETCHING

BEFORE SKETCH IS PREPARED, PIPING SYSTEMS SELECTED FOR ANALYSIS SHOULD BE REVIEWED WITH PIPING FLEXIBILITY GROUP FOR DETAILED INSTRUCTIONS ON INFORMATION REQUIRED. THE DATA BLOCK SHOULD BE COMPLETED WITH A SINGLE-LINE ISOMETRIC INCLUDING THE FOLLOWING MINIMUM INFORMATION:

1. MAXIMUM TEMPERATURE DIFFERENTIALS, CONSIDERING STEAM OUT, TRACING, STARTUP AND SHUTDOWN CONDITIONS.
2. ALL ANCHOR LOCATIONS; TERMINATION OF ALL PIPE MUST BE AT ANCHOR OR FIXED EQUIPMENT.
3. ALL FLANGES, WITH LOCATION AND WEIGHT.
4. VALVE WEIGHT AND LENGTH; INCLUDE WEIGHT OF MATING FLANGES.
5. REFERENCE TO NEAREST BUILDING COLUMN LINE.
6. ALSO GIVE AT LEAST ONE FLOOR ELEVATION.
7. SET PRESSURE AND ORIFICE SIZE OF RELIEF VALVES AND RUPTURE DISCS.
8. ALL PIPING DIMENSIONS TO THE NEAREST 1 INCH.
9. FOR VESSELS: OUTSIDE DIAMETER, WALL THICKNESS, MATERIAL OF CONSTRUCTION, DESIGN PRESSURE, OPERATING TEMPERATURE, NOZZLE THICKNESS AND VESSEL SUPPORT OR ANCHOR POINTS.
10. FOR PUMPS TO BE SPRING MOUNTED: PUMP WEIGHT, MOTOR WEIGHT, AND BED PLATE WEIGHT, WIDTH AND LENGTH.
11. ALLOWABLE MOMENTS AND FORCES ON TURBINES, COM-PRESSORS OR PUMPS.

INSTRUCTIONS FOR CONSTRUCTION

1. THIS DRAWING IS TO BE USED ONLY FOR SPRING HANGER, ANCHOR AND SUPPORT INSTALLATION. IT IS NOT TO BE USED FOR PIPE FABRICATION DETAILING.

2. FOR SPRING SIZES, LOADS, AND GENERAL INFORMATION, SEE W 1102.

3. NO OTHER SUPPORTS ARE TO BE ADDED WITHOUT DESIGN APPROVAL.

4. SUPPORTS MAY BE LOCATED ± 6" UNLESS NOTED.

5. REMOVE ALL TEMPORARY SUPPORTS BEFORE STARTUP.

GENERAL NOTES

1. FLEXIBILITY CALCULATIONS BASED ON 225 °F.

THIS DRAWING CONTAINS INFORMATION RELATING TO ACTIVITIES OF THE U.S. DEPARTMENT OF ENERGY. NOT TO BE REPRODUCED OR RELEASED WITHOUT PRIOR APPROVAL.

DATE: 10/1/80

BY: [Signature]

FOR: PIPING FLEXIBILITY ANALYSIS

SAVANNAH RIVER PLANT

BLDG. 24/H REPLACE WASTE HDR

W1102 & 1103 221H-HPPS & HPP6

PIPING FLEXIBILITY ANALYSIS

SHEET NO. 4

PROJECT: 25.1365

SCALE: NONE

DRAWN: L. TEMPERT

CHECKED: E. UYANAL

APPROVED: [Signature]

DATE: 10/1/80

W 712648

LAST REV. 2

REV. 1









ANALYZE FOR SAFETY, ECOLOGY AND MINIMUM ESSENTIAL DESIGN

BILL OF MATERIAL				NO. OF	
ITEM NO.	NAME	MATL.	SIZE	REMARKS	QTY.
1	CONNECTOR BLOCK	D 138617-B			1
2	CONNECTOR ASSEMBLY	W284777-ASSY-4			1
3	GASKET	SS-2-6719-A			1
4	CONNECTOR BLOCK	D 138617-B			1
5	CONNECTOR ASSEMBLY	W284777-ASSY-4			1
6	GASKET	SS-2-6719-A			1
7	LIFTING EYE	D 137753-A			1
8	BALL SWIVEL	D 137752-L			1
9	SNAP RING	D 11040-A			2

NOTES

- GENERAL
- SIZE PIPE AND OTHER MATERIAL, FABRICATOR, TESTING, ETC. FROM 3" TO 48" SHALL BE IN ACCORDANCE WITH THE SPECIFICATION 4482, SECTION P PARAGRAPHS P-53 AND P-54. SIZE PIPE AND OTHER SHALL BE IN ACCORDANCE WITH SPECIFICATION 4482, SECTION P PARAGRAPHS P-52, UNLESS OTHERWISE NOTED.
- PIPEING BROUGHT WITHIN TOLERANCES BY BENDING MUST BE MADE IN SUCH A MANNER THAT NO LOW SPOTS (POCKETS) EXIST WHEN THE PIPE IS IN THE INSTALLED POSITION.
- IT IS PERMISSIBLE TO MACHINE A MAXIMUM OF 1/4" OF METAL FROM THE CONNECTOR BLOCK FACE IN ORDER TO MEET FINISH OR TOLERANCE SPECIFICATIONS.
- WHEN A NEW TUBE IS SPECIFIED CASE MUST BE TAKEN WHEN WELDING THE TUBE TO THE FACE OF THE CONNECTOR BLOCK NOT TO EXCEED THE 3" I.D. OF THE MATING NOZZLE.

- SHIP FABRICATION
- JUMPER SHALL BE FABRICATED WITHIN THE TOLERANCE LIMITS, BASED ON AN AMBIENT TEMPERATURE AS STATED BELOW.
- CONNECTOR BLOCK FACES SHALL BE MAINTAINED PARALLEL TO THE AXIS OF PIPE TO WHICH THEY ARE WELDED TO WITHIN 1/8" - 3/16".
- ALL DIMENSIONS TO WITHIN 1/8" - 3/16".
- DIMENSIONS THAT LOCATE THE DISTANCE BETWEEN CONNECTOR BLOCKS IN THE X, Y AND Z GEOMETRIC PLANES SHALL BE MAINTAINED TO WITHIN 1/8".
- FIT-UP IN MOCK-UP OR JO

- JUMPER SHALL BE ALLOWED SUCH THAT WITH ONE CONNECTOR BLOCK BETWEEN THE JUMPER AND THE OTHER CONNECTOR BLOCK, THE OTHER BLOCK IS ALLOWED TO ITS CORRESPONDING FLANGE SO THAT:
- IN THE X, Y AND Z GEOMETRIC PLANES, THE JUMPER SHALL BE MAINTAINED PARALLEL BETWEEN THIS BLOCK AND FLANGE FACE IS WITHIN .010" IN 4".

- BAILING
- EXTERNAL BAILING FOR REMOTE HANDLING (BAIL) SHALL BE FABRICATED OF A166 TYPE 304 STAINLESS STEEL AND WELDED IN ACCORDANCE WITH THE SPECIFICATION 4482, SECTION P PARAGRAPHS P-53 AND P-54. THE JUMPER SHALL BE IDENTIFIED BY TRACK WELDING TWO 3" WIDE A166 TYPE 304 STAINLESS STEEL SHEETS ON THE JUMPER TO SUCH A POSITION THAT THEY CAN BE EASILY OBSERVED BY A REMOTE OPERATOR. THE JUMPER SHALL BE IDENTIFIED BY TRACK WELDING TWO 3" WIDE A166 TYPE 304 STAINLESS STEEL SHEETS ON THE JUMPER TO SUCH A POSITION THAT THEY CAN BE EASILY OBSERVED BY A REMOTE OPERATOR. THE JUMPER SHALL BE IDENTIFIED BY TRACK WELDING TWO 3" WIDE A166 TYPE 304 STAINLESS STEEL SHEETS ON THE JUMPER TO SUCH A POSITION THAT THEY CAN BE EASILY OBSERVED BY A REMOTE OPERATOR.

- IDENTIFICATION
- ASSEMBLY SHALL BE IDENTIFIED BY TRACK WELDING TWO 3" WIDE A166 TYPE 304 STAINLESS STEEL SHEETS ON THE JUMPER TO SUCH A POSITION THAT THEY CAN BE EASILY OBSERVED BY A REMOTE OPERATOR. THE JUMPER SHALL BE IDENTIFIED BY TRACK WELDING TWO 3" WIDE A166 TYPE 304 STAINLESS STEEL SHEETS ON THE JUMPER TO SUCH A POSITION THAT THEY CAN BE EASILY OBSERVED BY A REMOTE OPERATOR. THE JUMPER SHALL BE IDENTIFIED BY TRACK WELDING TWO 3" WIDE A166 TYPE 304 STAINLESS STEEL SHEETS ON THE JUMPER TO SUCH A POSITION THAT THEY CAN BE EASILY OBSERVED BY A REMOTE OPERATOR.

- "AS BUILT"
- DIMENSIONS SHOWN IN RECTANGULAR BLOCKS ARE "AS BUILT" AND DIMENSIONS SHOWN IN CIRCULAR BLOCKS ARE "AS BUILT" AND DIMENSIONS SHOWN IN TRIANGULAR BLOCKS ARE "AS BUILT".

SAVANNAH RIVER PLANT  
BLDG 241H  
PROCESS JUMPER  
ASSY IDENT NO. 2(HPP5) 15  
PROCESS EN.Y520-1-6-2  
LHW FROM CANYON TO P15

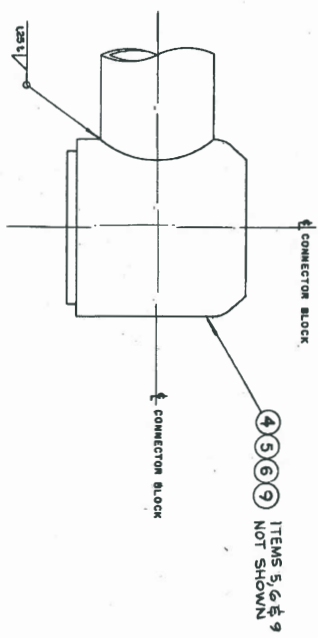
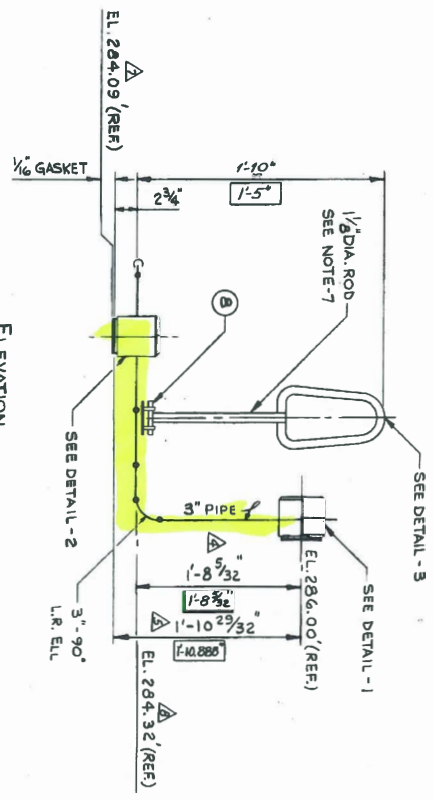
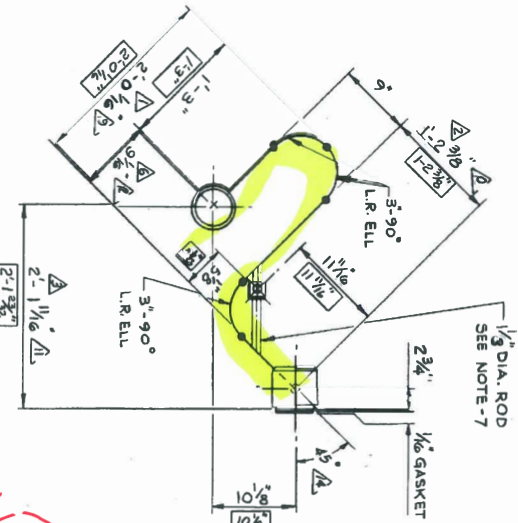
DATE	REVISION	DESCRIPTION
10/1/85	1	ISSUED FOR FABRICATION
10/1/85	2	ISSUED FOR FABRICATION
10/1/85	3	ISSUED FOR FABRICATION
10/1/85	4	ISSUED FOR FABRICATION
10/1/85	5	ISSUED FOR FABRICATION
10/1/85	6	ISSUED FOR FABRICATION
10/1/85	7	ISSUED FOR FABRICATION
10/1/85	8	ISSUED FOR FABRICATION
10/1/85	9	ISSUED FOR FABRICATION
10/1/85	10	ISSUED FOR FABRICATION
10/1/85	11	ISSUED FOR FABRICATION
10/1/85	12	ISSUED FOR FABRICATION
10/1/85	13	ISSUED FOR FABRICATION
10/1/85	14	ISSUED FOR FABRICATION
10/1/85	15	ISSUED FOR FABRICATION
10/1/85	16	ISSUED FOR FABRICATION
10/1/85	17	ISSUED FOR FABRICATION
10/1/85	18	ISSUED FOR FABRICATION
10/1/85	19	ISSUED FOR FABRICATION
10/1/85	20	ISSUED FOR FABRICATION
10/1/85	21	ISSUED FOR FABRICATION
10/1/85	22	ISSUED FOR FABRICATION
10/1/85	23	ISSUED FOR FABRICATION
10/1/85	24	ISSUED FOR FABRICATION
10/1/85	25	ISSUED FOR FABRICATION
10/1/85	26	ISSUED FOR FABRICATION
10/1/85	27	ISSUED FOR FABRICATION
10/1/85	28	ISSUED FOR FABRICATION
10/1/85	29	ISSUED FOR FABRICATION
10/1/85	30	ISSUED FOR FABRICATION
10/1/85	31	ISSUED FOR FABRICATION
10/1/85	32	ISSUED FOR FABRICATION
10/1/85	33	ISSUED FOR FABRICATION
10/1/85	34	ISSUED FOR FABRICATION
10/1/85	35	ISSUED FOR FABRICATION
10/1/85	36	ISSUED FOR FABRICATION
10/1/85	37	ISSUED FOR FABRICATION
10/1/85	38	ISSUED FOR FABRICATION
10/1/85	39	ISSUED FOR FABRICATION
10/1/85	40	ISSUED FOR FABRICATION

DATE 10/1/85  
BY 10/1/85

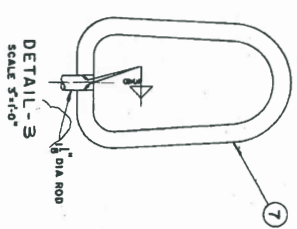
THIS DOCUMENT CONTAINS INFORMATION RELATING TO ACTIVITIES OF THE U.S. DEPARTMENT OF ENERGY. NOT TO BE REPRODUCED OR RELEASED WITHOUT PRIOR APPROVAL.

- NOTES: (CONT.)
- 7-MATL: ALL BAR & PLATE STOCK S. ST. GRADE 304L PER DUPONT SPEC. 4498
  - 8-WELDING: S. ST. TO S. ST. PER DUPONT SPEC. SW17W.
  - 9-ADDED AS BUILT DIMENSIONS

WF 1102



DETAIL - 2



NO.	DATE	REVISION	DESCRIPTION
1	10/1/85	1	ISSUED FOR FABRICATION
2	10/1/85	2	ISSUED FOR FABRICATION
3	10/1/85	3	ISSUED FOR FABRICATION
4	10/1/85	4	ISSUED FOR FABRICATION
5	10/1/85	5	ISSUED FOR FABRICATION
6	10/1/85	6	ISSUED FOR FABRICATION
7	10/1/85	7	ISSUED FOR FABRICATION
8	10/1/85	8	ISSUED FOR FABRICATION
9	10/1/85	9	ISSUED FOR FABRICATION
10	10/1/85	10	ISSUED FOR FABRICATION
11	10/1/85	11	ISSUED FOR FABRICATION
12	10/1/85	12	ISSUED FOR FABRICATION
13	10/1/85	13	ISSUED FOR FABRICATION
14	10/1/85	14	ISSUED FOR FABRICATION
15	10/1/85	15	ISSUED FOR FABRICATION
16	10/1/85	16	ISSUED FOR FABRICATION
17	10/1/85	17	ISSUED FOR FABRICATION
18	10/1/85	18	ISSUED FOR FABRICATION
19	10/1/85	19	ISSUED FOR FABRICATION
20	10/1/85	20	ISSUED FOR FABRICATION
21	10/1/85	21	ISSUED FOR FABRICATION
22	10/1/85	22	ISSUED FOR FABRICATION
23	10/1/85	23	ISSUED FOR FABRICATION
24	10/1/85	24	ISSUED FOR FABRICATION
25	10/1/85	25	ISSUED FOR FABRICATION
26	10/1/85	26	ISSUED FOR FABRICATION
27	10/1/85	27	ISSUED FOR FABRICATION
28	10/1/85	28	ISSUED FOR FABRICATION
29	10/1/85	29	ISSUED FOR FABRICATION
30	10/1/85	30	ISSUED FOR FABRICATION
31	10/1/85	31	ISSUED FOR FABRICATION
32	10/1/85	32	ISSUED FOR FABRICATION
33	10/1/85	33	ISSUED FOR FABRICATION
34	10/1/85	34	ISSUED FOR FABRICATION
35	10/1/85	35	ISSUED FOR FABRICATION
36	10/1/85	36	ISSUED FOR FABRICATION
37	10/1/85	37	ISSUED FOR FABRICATION
38	10/1/85	38	ISSUED FOR FABRICATION
39	10/1/85	39	ISSUED FOR FABRICATION
40	10/1/85	40	ISSUED FOR FABRICATION

SAVANNAH RIVER PLANT  
BLDG 241H  
PROCESS JUMPER  
ASSY IDENT NO. 2(HPP5) 15  
PROCESS EN.Y520-1-6-2  
LHW FROM CANYON TO P15



**Distribution:**

[cj.bannochie@srnl.doe.gov](mailto:cj.bannochie@srnl.doe.gov)  
[William.bates@srnl.doe.gov](mailto:William.bates@srnl.doe.gov)  
[marion.cofer@srnl.doe.gov](mailto:marion.cofer@srnl.doe.gov)  
[alex.cozzi@srnl.doe.gov](mailto:alex.cozzi@srnl.doe.gov)  
[connie.herman@srnl.doe.gov](mailto:connie.herman@srnl.doe.gov)  
[brady.lee@srnl.doe.gov](mailto:brady.lee@srnl.doe.gov)  
[Joseph.Manna@srnl.doe.gov](mailto:Joseph.Manna@srnl.doe.gov)  
[Gregg.Morgan@srnl.doe.gov](mailto:Gregg.Morgan@srnl.doe.gov)  
[frank.pennebaker@srnl.doe.gov](mailto:frank.pennebaker@srnl.doe.gov)  
[William.Ramsey@srnl.doe.gov](mailto:William.Ramsey@srnl.doe.gov)  
[Marissa.Reigel@srnl.doe.gov](mailto:Marissa.Reigel@srnl.doe.gov)  
[eric.skidmore@srnl.doe.gov](mailto:eric.skidmore@srnl.doe.gov)  
[michael.stone@srnl.doe.gov](mailto:michael.stone@srnl.doe.gov)  
[william.swift@srnl.doe.gov](mailto:william.swift@srnl.doe.gov)  
[Boyd.Wiedenman@srnl.doe.gov](mailto:Boyd.Wiedenman@srnl.doe.gov)

Records Administration (EDWS)

[Catherine.Mussi@srnl.doe.gov](mailto:Catherine.Mussi@srnl.doe.gov)  
[David.Herman@srnl.doe.gov](mailto:David.Herman@srnl.doe.gov)  
[jonathan.duffey@srnl.doe.gov](mailto:jonathan.duffey@srnl.doe.gov)  
[matthew.mills@srnl.doe.gov](mailto:matthew.mills@srnl.doe.gov)  
[chris.martino@srnl.doe.gov](mailto:chris.martino@srnl.doe.gov)

[steven.brown@srs.gov](mailto:steven.brown@srs.gov)  
[james.therrell@srs.gov](mailto:james.therrell@srs.gov)  
[kenneth.burrows@srs.gov](mailto:kenneth.burrows@srs.gov)  
[kevin.usher@srs.gov](mailto:kevin.usher@srs.gov)  
[tara.smith@srs.gov](mailto:tara.smith@srs.gov)  
[nina.vinci@srs.gov](mailto:nina.vinci@srs.gov)  
[mark.hudlow@srs.gov](mailto:mark.hudlow@srs.gov)  
[Eloy.Saldivar@srs.gov](mailto:Eloy.Saldivar@srs.gov)  
[Jacob.mellon@srs.gov](mailto:Jacob.mellon@srs.gov)  
[omar.rodriquez@srs.gov](mailto:omar.rodriquez@srs.gov)  
[matthew.arnold@srs.gov](mailto:matthew.arnold@srs.gov)  
[mackenzie.yerger@srs.gov](mailto:mackenzie.yerger@srs.gov)  
[William.dyer@srs.gov](mailto:William.dyer@srs.gov)  
[robert.gunby@srs.gov](mailto:robert.gunby@srs.gov)  
[daniel.tenpenny@srs.gov](mailto:daniel.tenpenny@srs.gov)  
[terri.fellinger@srs.gov](mailto:terri.fellinger@srs.gov)  
[maria.rios-armstrong@srs.gov](mailto:maria.rios-armstrong@srs.gov)  
[vijay.jain@srs.gov](mailto:vijay.jain@srs.gov)